[UCI]I804:24011-200000267555

2019 년 8 월
석박사학위 논문

폴리머 공기예열기의 열유동 해석

조선대학교 대학원

기 계 공 학 과

NGOC VI NGUYEN

폴리머 공기예열기의 열유동 해석

NUMERICAL ANALYSIS OF POLYMER ROTARY REGENERATOR

2019 년 8 월 23 일

조선대학교 대학원

기 계 공 학 과

NGOC VI NGUYEN

폴리머 공기예열기의 열유동 해석

지도교수 오 동 욱

이 논문을 공학석사 학위신청 논문으로 제출함

2019 년 4 월

조선대학교 대학원

기 계 공 학 과

NGOC VI NGUYEN

NGOC VI NGUYEN 의 석사학위논문을 인준함

위원장 조선대학교 교수 조 홍 현 (인)

위 원 조선대학교 교수 박 정 수 (인)

위 원 조선대학교 교수 오 동 욱 (인)

2019 년 5 월

조선대학교 대학원

CONTENTS

LIST OF FIGURES

List of Tables

NOMENCLATURE

L : Length of plate [m]

d : flow channel thickness [m]

z : wall thickness [m]

x, y : Cartesian coordinate

ρ : density [kg/m^3]

c_p : specific heat capacity [kJ/(kg.K)]

λ : thermal conductivity [W/(m.K)]

A : cross-section area [m^2]

T : temperature [°C]

t : time [s]

h : convective heat transfer coefficient [W/(m^2.K)]

P : perimeter of geometry [m]

v : velocity [m/s]

$\mathbf{u}$: velocity field [m/s]

Re : Reynolds number

Nu : Nusselt number

S : sensitivity parameter

p_A : absolute pressure [Pa]

$\mathbf{n}$: normal vector

Subscripts

h : hot

c : cold

m : wall surface

w : matrix wall

f : fluid

i : inlet

o : outlet

Greeks

alpha : thermal diffusivity

μ : dynamic viscosity [kg/(m.s)]

ε : effectiveness

ABSTRACT

Numerical Analysis of Polymer Rotary Regenerator

NGOC VI NGUYEN
Advisor: Prof. DONG-WOOK OH,
Department of Mechanical
Engineering, Graduate School of
CHOSUN University.

The corrosive characteristic of flue gas to metal rotary regenerator (RR) working in thermal power plant gained its gravity many years ago. In this study, the RR made of polymer, as known as a highly corrosive resistant material, is applied and experiences a comparison of heat exchanger efficiency to metal. Those materials are polytetrafluoroethylene (PTFE), polyether ether ketone (PEEK), perfluoroalkoxy alkanes (PFA), aluminum (Al) and corrosive resistant low alloy steel (CRLS). The 2D computational fluid dynamic (CFD) model are established and their numerical results are validated with available literatures. There are also two mathematical configurations which are applied in this study. The first one is a simple model with equations of one – dimensional (1D) fluid flow and two – dimensional (2D) wall. The flow characteristic for both fluid flows is considered as laminar by uniform and constant inlet velocity. Heat transfer coefficients along with length of the plate are figured out from a Nusselt empirical correlation and put in the fluid flow equations. After checking the condition

of energy conversation, the heat exchanger effectiveness depending on either variable wall or flow channel thicknesses of those materials has compared each other. For the second one, although the fluid flow is laminar, mathematical model is chosen as transient weakly compressible turbulent forced convection in channel. A range of different mass flow rate is also put at inlet condition for both fluid flow. The energy equations of fluid flow and matrix wall (solid region) are also transient heat convection and conduction. The results of Nu number and effectiveness of present study are validated with empirical correlations and analytical solution ε_NTU method, respectively. For both mathematical models, they are coupled and solved by finite element method from COMSOL Multiphysics. The influence of different Reynold numbers and thickness of matrix wall and flow channel on the rotary regenerator's behavior has also been examined. As a consequence, the comparable quantity of effectiveness, under 10% of difference, is witnessed between two kinds of material. The narrower the flow channel is, the higher the effectiveness is. Otherwise, wall thickness influences weakly to heat exchanger effectiveness. Eventually, a sensitivity analysis of those materials is performed based on the light change of thermal conductivity and volumetric heat capacity to test its influence on the total effectiveness. Conclusively, materials with larger thermal mass are more desirable than those with higher thermal conductivity.

I. Introduction

A. Definition of rotary regenerator

Energy is an indispensable thing in the modern life nowadays. The oil crisis in 1973 was like a bell to wake the developing countries around the world up and brought to an inevitable truth that their economy depended a lot on finite fossil fuel resources. To maintain the energy security and economic development, a large number of researches were required to stand against this crisis and recommended an effective way to manage well an energy use in commercial – industrial purposes. As a result, each specific application has its own solution. Natural gas, nuclear power and clean energy such as wind, solar, geothermal and so on were offered to be alternative fuels. Additionally, cope with the living – environmental devastation caused by using coal in thermal power plants (TPP) while upgrading its efficiency still remained intractable. So, energy storage devices gained their importance in improving the overall performance as well as declined the energy consumption through utilizing the waste heat recovery.

There are many energy storage units with a wide range of their function; however, this study focuses on the thermal one. In spectacular, it is rotary regenerator and usually applied in thermal power plant. There are two outlooks on analyzing the thermal regenerator. Firstly, by being a regenerative heat exchanger, a porous media is seen as a permeable packing (a packing is formed by a large number of matrix walls) which is used for storing the heat from hot fluid flow and then releasing it to the cooler one. This way looks efficient due to maximizing the absorption of thermal energy from hot fluid, then transferring it to the cooler fluid. During a cycle known as hot period, whole surface area of the heat exchanger is occupied by the hot fluid flow and obviously keep the sensible heat up in the matrix walls. After a constant time, hot period ends and is replaced by a switch in which the cooler fluid flow begins passing through the same channels created by matrix walls. The sensible heat stored in the packing before is released to the cooler flow during cold period. Once finished, a full closed cycle has been done for a

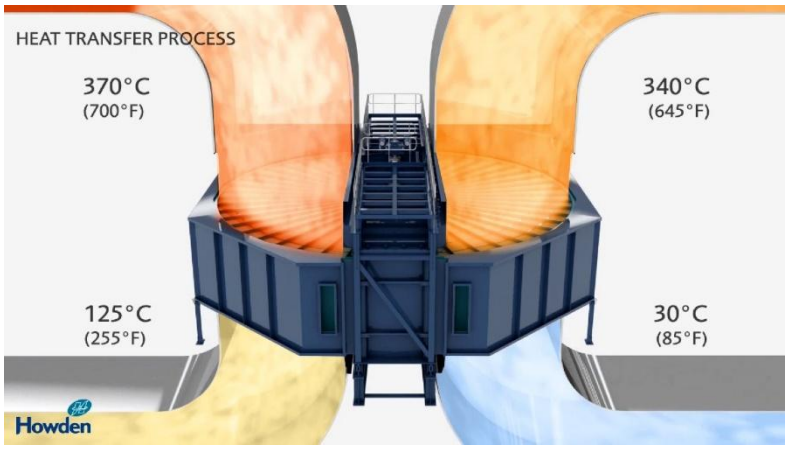

Fig. I. 1. Typical rotary regenerator in thermal power plant

certain length of time and usually known as a cycle of operation. Secondly, the simpler way to view this heat exchanger is that its packing is dealt with a succession of linked single blows. It means the sensible heat from hot flow is accumulated inside matrix walls until the hot period and subsequently recovered in the time of cold period. In order to minimize the heat after being stored in the packing not come back from the hot flow while still fulfilling the thermal requirement of cold period, a certain time of full cycle (including hot and cold periods) should be chosen reasonably. Moreover, it also could help in manipulating the thermal performance of this regenerative heat exchanger to meet the prescribed operating conditions. Cycle operation is one of the characteristics of regenerator. The temperature profile in one cycle is analogous to that in the next, meaning that the thermal regenerator has passed many cycles of identical operation. At that time, an equilibrium state which often known as periodic steady state is reached – temperature oscillation no longer is a function of time. Step change could often be proposed to the operating parameters. Specifically, they are inlet fluid temperature and mass flow rate, either hot or cold periods. The regenerator is going to restart with experiencing a number of transient cycles until a new cyclic equilibrium is reached. There are two common flow configurations encountered in the heat exchanger. The first one is counter flow operation which the hot and cold fluids come in opposite direction;

they also could flow alternatively in the rotary regenerator. This model is seen as the most effective one in comparison with the parallel flow – the second one. Like its name, those two fluid flows pass through the packing of heat exchanger either same time or by turns, depending on what kinds of heat exchanger are. At the real operating conditions, the hot fluid is asked, the discontinuous operation of the regenerator which apparently must be accounted for, could be disguise in the theoretical study.

As known, a heat exchanger which performs the heat recirculation between the inlet fresh air and exhaust flue gas is applied to recover wasted thermal energy instead of discharging it to the outside. One of those, a recuperator – heat exchanger happens in a direct transfer way by separating fluids and heat transfer surface, also do not leak or mix each other. The another one is referred to as indirect transfer way, a regenerator exchanges heat periodically between hot – cold fluids via thermal energy storage. The regenerator is divided into two types depending on their application in each industry: fixed-bed and rotary. Because of the simple flow structure and ease of maintenance, rotary regenerator is commonly applied in TPP. Ljungstrom and Rothemuhle are two popular types of rotary heat exchanger. Ljungstrom rotary regenerator contains a large number of matrix walls which are often shaped by sinusoid curves and bent to create a cylindrical packing (or matrix core). In the packing, small spaces between each of two matrix walls are established and named as fluid channels. Whole surface area of walls is used for absorbing the sensible heat from the hot fluid and then releasing it to the cooler one. An axis put in the middle of this equipment allows the cylindrical packing to rotate continuously between a constant segment of hot and cold periods. At a fixed direction, the exhaust gas passes through, the core submerged inside this hot stream absorbs heat. Then, on the moving of rotation, this heat is released to the remaining segment of the cold stream which flows in inverse direction to the hot one during ending a cycle. The operation of a rotary regenerator eventually achieves a steady periodic state, wherein a cyclic equilibrium is achieved as the temperature in the exchanger medium and the outlet temperatures of the fluids do not vary among successive cycles. These

comparable physical effect is also recognized in the Rothemuhle design. However, the rotor and stator are reversal compared to the Ljungstrom. The matrix core is kept as stationary while hot and cold fluids are achieved by rotating alternatively around the distributing hoods, which are put on the top and bottom faces of matrix core. The remarkable point which needs to be paid more attention is handling the air leakage between two segments of hot and cold flows, at the entrance and exit faces of rotary regenerator. By subjectively observing the thermal regenerator, at here is rotary form, it shall be commented that the switching from the hot/cold to the cold/hot flows by rotating of cylindrical packing beneath gas seals for both rotary arrangements is essential. Nevertheless, it is completely reverse and may be considered as a nuisance. Hausen offers that in an ideal case, a regenerator should be applied where the power plant in which it is assembled operates in periodic behavior. This is hardly obtained. However, the pros is bringing the alternative hot and cold flows through the same passages in the packing. Based on the other stream, dirt contained in one stream can be purged, hence avoiding the obstruction of the flow channels.

The material for this equipment should be chosen based on some following characteristics such as high volume heat capacity (the product of density and specific heat capacity), high thermal conductivity, high melting temperature to sustain reversible heating and cooling, chemical and geometrical stability, noncombustible, noncorrosive, nontoxic, low cost and ease for fabrication, sufficient mechanical strength. However, there are no single material which could meet all these standards. Depending on each application, the engineer shall choose the most appropriate material. Traditionally, the material used for fabricating of rotary regenerator is metal, which is well-known for its high thermal conductivity as well as coefficient of thermal expansion (CTE). Besides, owning high melting temperature allows metal to work under a wide range of harsh condition, especially in TPP. The serious issue of rotary regenerator on coal power plant is usually connected with corrosion caused by the appearance to either sulfuric acid or water dew point. There are two options which could be used to minimize this point.

Normally, the matrix core is going to be covered by anti-corrosive enamel. Another way is to apply the polymer in fabricating the regenerator. As known, the thermal conductivity and volumetric heat capacity (which is calculated as the product of density and heat capacity) of, for example, polyether ether ketone (PEEK) are 1.5% and 56%, respectively, lower than those of stainless steel. With the essence of direct heat transfer, thermal conductivity plays an important role for recuperator and hence, metal is usually a better choice than polymer. In contrast, regenerator with indirect heat transfer requires high porosity, low solid volume of matrix core. In order to store heat as much as possible, the high volumetric heat capacity ($\rho_w c_{pw}$) is desired for the matrix core. Therefore, polymer which inherently has low thermal conductivity, high volumetric heat capacity, anti – corrosive and light weight is possible to become a material for manufacturing rotary regenerator. The following table and graphs illustrate the potential polymer and their properties which could be applied in this field.

Many theoretical studies about thermal storage and regenerative heat exchanger are performed and summarized in the books of Schmidt and Willmott [ ]. The geometry of storage packing does not need to be specify except to the case that matrix core is seen as porous media. Commonly, the heat storage unit is shaped to the rectangular, circular or sinusoidal flow passages. The simplest condition is figured out when the matrix walls is at a uniform temperature and the fluid is also at the same temperature. Then the fluid is attributed to a single step change in temperature and the fluid flow rate still remains unchangeable. The storage unit is realized to be operating under single-blow conditions. In this single blow problem, they report two mathematical models to estimate thermal energy of concerned parameters: infinite fluid heat capacity (fluid temperature is assumed to be constant), simplified finite conductivity model with an analysis of the effect of longitudinal and latitudinal conductions. Next, the elementary definition of counterflow thermal regenerator is establish as long as its mathematical modelling. Based on linear characteristic, this model has been assumed that the heat transfer coefficient is simple convective surface coefficient and hence, it is necessary to figure

out how to calculate the lumped coefficient correctly. The influence of operating cycle and periodic steady state is presented. To solve the differential equations of counterflow regenerator, two methods have elected among a lot of published solutions. The first one is open method where the model of regenerator reaches an energy equilibrium after a number of cycles and the another one is closed method in which periodic steady state is computed directly. By setting up the temperature dependence of any of the thermophysical properties, nonlinear model appears and is analyzed by several methods and operating parameters such as time varying factor, gas flow rate or inlet fluid temperature. The thermal capacity of matrix core has a fundamental limit that it is impossible to correspond urgently to any step change of inlet fluid temperature or flow rate in operation. Instead, a number of transient cycles need to be performed again until reaching the periodic steady state.

Tab. I. 1. Thermal properties of materials

Material	Density (kg/m^3)	Thermal Conductivity (W/m.K)	Melting Temperature (°C)	Coefficient of Thermal Expansion ($10^{-6}/K$)	Specific Heat Capacity (J/kg.K)	Thermal Diffusivity ($10^{-7}m^2/s$)
PPS (Polyphenylenesulfide)	1350	0.3	275 – 290	60	1000	22.2
PEEK (Polyetheretherketone)	1330	0.25	335 – 345	50 – 70	1700	11.1
PTFE (Polytetrafluoroethylene)	2170	0.27	325 – 335	100 – 150	1000	11
PVDF (Polyvinylidene fluoride)	1780	0.19	170 – 175	110 – 130	1400	9.1

PET (Polyethyleneterephthalate)	1390	0.24	245 – 260	80 – 100	1170	16.8
PSU (Polysulfone)	1245	0.15	332 – 371	50 – 60	1370	8.8
FEP (Tetrafluoroethylene)	2145	0.25	253 – 282	80	1120	10.4
ETFE (Ethylenetetrafluoroethylene)	1700	0.23	225 – 275	40	900	15
PVF (Polyvinyl fluoride)	1380	0.13	190 – 200	50 – 97	1400	6.7
PA6/3T (Polyamide 6/3T)	1120	0.23	290	80	1600	12.8
PA6/6T (Polyamide 6/6T)	1180	0.24	275	70	1570	13
PEI (Polyethylenimine)	1270	0.22	295 – 323	50	2000	8.7
PES (Polyethersulfone)	1370	0.18	343 – 377	60	1370	9.6
PFA (Perfluoroalkoxy)	2150	0.19	285 – 305	120	1172	7.5
PA11 (Polyamide 11)	1040	0.26	180 – 190	85 – 120	1260	19.5
PA12 (Polyamide 12)	1025	0.23	170 – 180	120 – 140	1215	18.5
PA46 (Polyamide 46)	1195	0.3	290 – 295	70 – 80	2100	12
PA6 (Polyamide 6)	1135	0.28	225 – 235	80 – 90	1645	14.7

PA610 (Polyamide 610)	1080	0.2	210 – 230	70 – 90	1600	11.6
PA612 (Polyamide 612)	1060	0.22	210 – 220	120 – 130	1910	10.9
PA66 (Polyamide 66)	1145	0.29	225 – 265	35 – 45	1685	14.8
PBT (Polybutylene terephthalate)	1310	0.27	220 – 230	80 – 100	1300	15.9
PET (Polyethylene terephthalate)	1290	0.24	245 – 260	80 – 100	1105	16.8
PC (Polycarbonate)	1220	0.2	225	75 – 80	1335	12.3
PMMA (Polymethylmethacrylate)	1170	0.21	230	90 – 110	1460	12
POM(copo) (Polyoxymethylene)	1410	0.27	140 – 170	110 – 150	1490	12.9
POM(homo) (Polyoxymethylene)	1410	0.34	175 – 190	160 – 180	1490	15.9

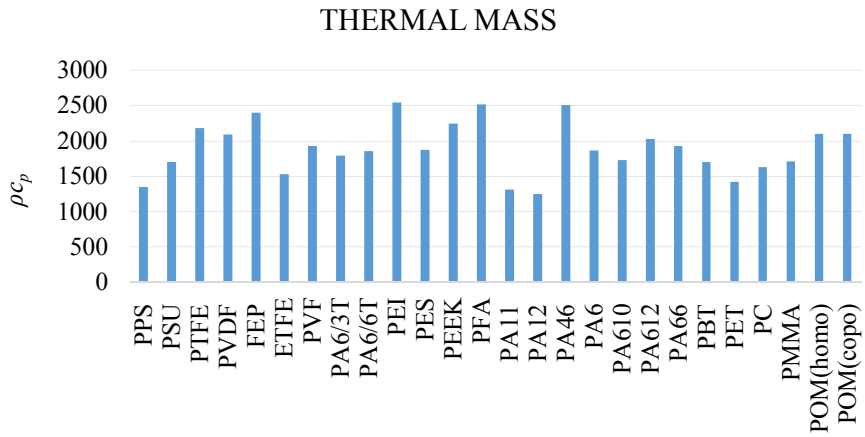

Fig. I. 2. Thermal mass of polymer materials

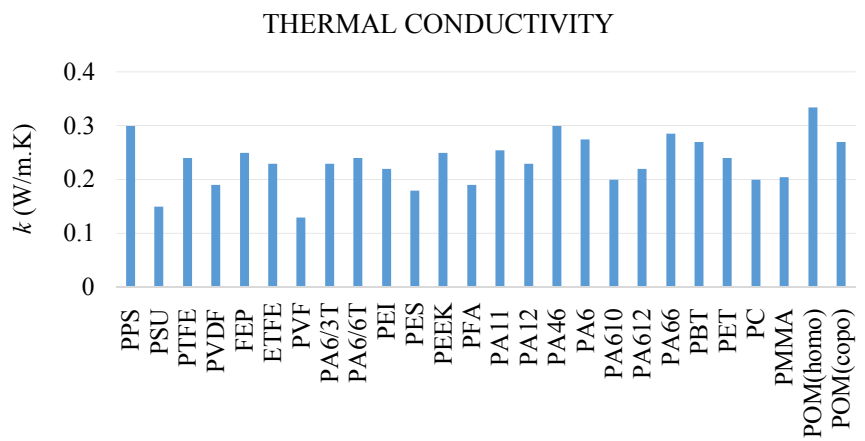

Fig. I. 3. Thermal conductivity of polymer materials

B. The typical published researches

Recently, many studies have been conducted for applying polymers and polymer composites to thermal systems. A polymer heat exchanger can be fabricated and maintained inexpensively and operated in extreme toxic environments, and the low density of the polymer material makes the system lightweight. Most previous studies focused on the application of polymeric materials to a recuperative heat exchanger, where the heat exchanger material lies in between hot and cold fluid flows. In such cases, the thermal resistance of the heat exchanger wall becomes an important design factor. Since the thermal conductivity of a polymer is two or three orders of magnitude smaller than that of metals, many studies have been conducted for increasing the thermal conductivity of a recuperative polymer heat exchanger with the aim of narrowing the thermal performance gap between metal and polymer heat exchangers [Chen (2009),]. Zaheed (2004) figures several kinds of polymers which could be used in compact heat exchanger such as PVDF, PTFE, PP and so on. Because of their relative merits, they become potential materials for a large range of either industrial and commercial applications presently dominated by metallic heat exchanger. For PVDF heat exchanger, the cost savings might be obtained remarkably when consolidating the same tube dimensions, thickness and fluid coefficients. A number of design aspects for polymer film compact heat exchanger such as thin films, corrugations, narrow channels and developing laminar flow are also emphasized. In additions, the fouling and corrosive resistances are probably the superiority in manufacture of heat exchanger especially applied in chemical industry. Trojanowski (2016) reports the polymer heat exchanger made of nylon-12, PP-based materials E1201 and RS1486, or copolyester (COPE) D4302 is applied to waste heat recover from hot flue gas exhausted by boiler. Compared to metal, the results show that the overall thermal performance of polymer could be obtained analogously by increasing roughly 10 times in thermal conductivity. Due to lower conductivity of polymer, the higher temperature is witnessed at the surface and

condensation rate is lower. If the boiler is burned by oil, latent heat accounts for a small percentage of heat recovered.

A large number of studies of rotary regenerator have been conducted since the 20th century. In the beginning, most researches focus on investigating the capability of heat and mass transfer. They apply either numerical or analytical solutions for solving relevant differential equations [Kern (1974), Schmidt (1983), San (1993), Nair (1998), Wang (2019)]. Zhang (2003) uses a one-dimensional mathematical model to investigate the heat and mass transfer of honeycombed rotary regenerator. Then, the results have been validated and fixed well with the experiment of a real desiccant wheel. They indicates that the air humidity ratio always appear at the hump curve and rise moderately until the hump ends at duct exit. The influence of regenerative, processing velocities and inlet fluid temperature are studied. Yilmaz (2003) published an analytical solution for estimating the effectiveness of rotary regenerator. It could be applied for many shapes of flow channel constituting the matrix core without the limit of rotational speed. Skiepko (2004) establishes a model of rotary regenerator which contains the influence of longitudinal conduction in energy equations. Then its results are compared and found to be approximately 3% in agreement with experimental data which is figured out from real operating air preheater. Sphaier (2004) develops a new mathematical model which describes specifically heat and mass transfer process occurred in porous sorbent of rotary regenerator. For validation, it is compared to a previous published experimental data. Despite the inevitable further research related to the effect of characteristic parameters on regenerative efficiency, this formulation could be used for calculating either enthalpy or desiccant wheel accurately. Moreover, the adaptation of this model is very flexible so some physical features can be added such as temperature dependent properties, supporting structure and considering entrance region for thermal and hydrodynamically of fluid flow. Monte (2008) publishes an accurate analytical solution for solving one-dimensional linear model of thermal regenerator operating at counterflow configuration. The heat transfer process is at cyclic steady state. Initially, the integral form of fluid

temperature is presented along the path of a gas particle, over different space and time intervals. The Organ's theory of independent flow regimes is applied to cope with gas particles in each solutions for hot, cold and internal fluids. Eventually, the closed form for the anticipation of regenerative effectiveness as a function of NTU and flush ratio is presented. Since there are still some issues happening with conventional dehumidified equipment, Yamaguchi (2013) performs the numerical and experimental analysis of rotary desiccant wheel which is the main component of desiccant air conditioning system. Under variable operating parameters, the theory model is calculated and evaluates the effect of entrance region in flow channel, the diffusion in porous solid. For experiments, the responses of regenerative fluid temperature and velocity, thickness and rotational speed of thermal packing to wheel efficiency are studied. At the exit of the wheel, fluid temperature and humidity distribution are calibrated. The results between theoretical model and experiment are generally in good agreement, with 10.8 % of temperature and 3.3 % of humidity ratio. To calculate the heat recovery by using rotary heat exchanger, Seo (2018) develops a simple effectiveness model. From governing equations of cyclic thermal regenerator at the steady state, an approximate solution is achieved and after that, it is used for formulating the effectiveness correlation. This one then is validated with available literatures and show the maximum tolerance of 5 %. Finally, the simple empirical correlations are introduced for practical purposes. The influence of leakage on flue gas parameter, purge sector, thermal performance or rotational speed on effectiveness of rotary regenerator was also considered sorely [Shah (1999), Buyukalaca (2002), Drobnic (2006), Yadav (2014)]. A method applied genetic algorithm to maximize the thermal efficiency and minimize the total pressure drop of rotary regenerator, as known as multi-objective optimization, was introduced [Sanaye (2009), Raja (2016), Wang (2019)]. You (2016) applied a numerical method called unsteady conjugate heat transfer between fluid flows and matrix core to simulate three dimensional (3D) ceramic regenerator, with the assumptions of laminar flow and negligible radiation. At here, the regenerator was constituted from 3D flow channels

which are small square openings and the calculation is based on one typical channel. As a result, the model matched well with experimental data. Decreasing the switching time of periods and air inlet velocity led to increase preheated air temperature, effectiveness and energy recover ratio. Porous media approach used by Ozdemir (2018) to simulate the 3D rotary heat exchanger was conducted. On the one hand, a single triangular channel was employed to achieve the porosity parameter and convective heat transfer coefficient. On the other hand, these parameter were applied to simulate a 3D cylinder representing for rotary heat exchanger with the round hole in the middle. Consequently, the less angular velocity and inlet hot gas temperature were, the better overall thermal performance could reach. Due to the well-known characteristics of polymer in heat exchanger, it was studied early by many researchers. Reay (1989) reported the merits and limitations of polymer in this field, concurrently its application in fabricating some kinds of heat exchanger such as gas – gas, gas – liquid and liquid – liquid. At that time, polymer was regularly used for shell and tube heat exchanger in acid plants. Although metal was protected by coating plastic to stand against corrosion resistance, polymer seemed more advantageous with the alleviation of fouling issue and weight. Dreiser (2016) presented an investigation of falling film break-up and thermal efficiency of polymer film heat exchanger. With the spacer grid, polymer films (25 μm) are offered to get the high convective heat transfer coefficient. Chung (2016) built an experiment as well as numerical model of plastic rotary regenerator. Their aim is to optimize design parameters such as rotating speed, split, aspect ratio and purge section angle.

C. Objectives and scope of the thesis

Although a constant number of researches related to rotary regenerator have been conducted, there is a limitation of documents concerning about those made of polymer. In this study, the sensible heat transfer characteristic of polymer used to replace for metal in rotary regenerator is figured out.

Part A is used for the validation between commercial code of COMSOL and empirical correlation performed by the previous researchers. The present mathematical model is conjugate heat transfer model with two – dimensional (2D) fluid and heat storage domains. The fluid is assumed as incompressible and belongs to laminar regime. After a number of iterations, the model reaches the periodic steady state and convection heat transfer coefficients are figured out to compare with Stephan's correlation. Since they are in well agreement, the Stephan correlation then is applied for the simple mathematical model with 1D fluid and 2D heat storage domains, established by Schmidt and Willmott in 1983.

Part B discusses about the difference of governing equations solved by previous researcher's finite difference method (FDM) and COMSOL's finite element method (FEM). By solving the finite conductivity model for single – blow problem, two numerical methods are roughly comparable. From this point of view, commercial code of COMSOL is proved to be reliable and used for the thermal evaluation of polymers.

In part C, the single-blow operation for two fluid flows is used for simulating the heat storage exchanger, known as the first model. The heat transfer mechanism of a rotary regenerator at here is modeled as air flows on a flat plate. Governing equations for the air flow and plate are established through application of the energy conservation law. The heat transfer rate and heat exchanger effectiveness under variation of the heat exchanger material, flow channel thickness, and heat exchanger wall thickness are calculated and compared. Additionally, a sensitivity analysis is performed to investigate the influence of the material thermal conductivity and thermal mass on the heat exchanger effectiveness.

In part D, the conjugate heat transfer model with full Navier-Stokes equations is replaced to evaluate polymer's thermal performance. The flow characteristics are assumed as turbulent (RANS type), weakly compressible. The model experiences a number of iterations before approaching the periodic steady state. From the results, convection heat transfer coefficients are validated with several correlations of published literatures. The effectiveness is also validated with analytical solution ε_NTU method.

In conclusion, with some pros and cons of polymer in comparison with metal, thermal fields of the regenerative model are still restricted among literatures. Hence, these things are an impulse on this investigation.

II. Model analysis

A. The estimation of heat transfer coefficient used in finite conductivity model

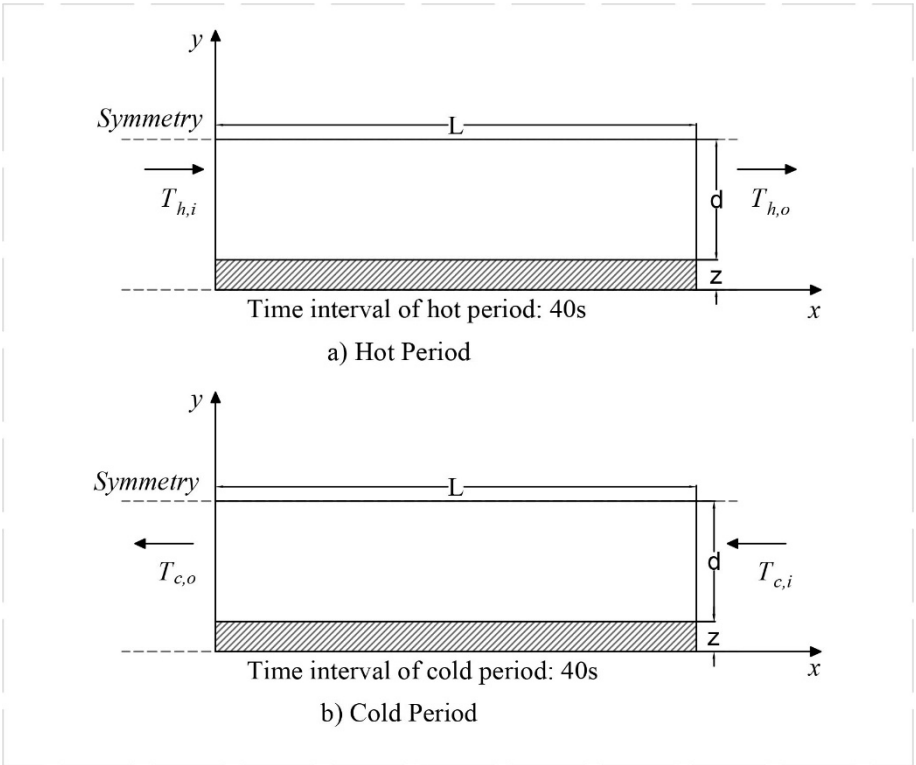

Fig. II. 1. Schematic of the calculated domains and boundary conditions

1. Governing equations

One of main parts of this study is based strongly on the theoretical models published by Schmidt and Willmott in 1981. They impose some assumptions on their model such as temperature independent of thermophysical properties for either fluid or solid, constant fluid velocity, and so on. However, the important thing which this part focuses, is the convection heat transfer coefficient. From these point of view, the non-isothermal flow and conjugate heat transfer interfaces are applied to predict the convection heat transfer coefficient as function of x - coordinate that is going to be used in Schmidt and

Willmott's model. Then, it is double checked with an empirical correlation of Stephan. The boundary conditions are described in fig. above. The flow at here is considered as incompressible, laminar and its thermal properties are temperature independence and chosen at initial inlet temperature of fluid. The distribution of initial temperature in solid is uniform. Following tables show related parameters used in this model.

Tab. II. 1 The operating details of rotary regenerator

Parameter	Unit	Expression
L	mm	400
d	mm	6
z	mm	0.6
t_h	s	40
t_c	s	40
$T_{h,i}$	°C	150
$T_{c,i}$	°C	30
$T_{s,\,initial}$	°C	25
$\boldsymbol{v}_{h,i}$	m/s	1
$\boldsymbol{v}_{c,i}$	m/s	1

Tab. II. 2 Thermal properties of calculated materials

	Unit	Al	PTFE	PEEK
ρ_w	kg/m^3	2700	2180	1320
c_{pw}	J/kg·K	900	1050	1700
k_w	W/m·K	238	0.24	0.25

Tab. II. 3 Thermal properties of hot and cold fluid flows

Property	Unit	Expression
$\mu_{f,h}$	kg/m·s	2.322E-5
$\mu_{f,c}$	kg/m·s	1.9175E-5
$\rho_{f,h}$	kg/m^3	0.8661
$\rho_{f,c}$	kg/m^3	1.128
$c_{pf,h}$	J/kg·K	1012.15
$c_{pf,c}$	J/kg·K	1007
$k_{f,h}$	W/m·K	0.033388
$k_{f,c}$	W/m·K	0.026615

- The continuity equation is written as:

$$\nabla \cdot (\rho_f \mathbf{u}) = 0 \quad (1)$$

- The momentum equation:

$$\rho_f \frac{\partial \mathbf{u}}{\partial t} + \rho_f (\mathbf{u} \cdot \nabla)\mathbf{u} = -\nabla \cdot \mathrm{p} + \nabla \cdot [\mu(\nabla \mathbf{u} + (\nabla \mathbf{u})^{\mathrm{T}} - \frac{2}{3}\mu(\nabla \cdot \mathbf{u})\boldsymbol{I} \quad (2)$$

- The energy equations of fluid and solid :

$$(\rho c_p)_f \left[\frac{\partial T}{\partial t} + (\mathbf{u} \cdot \nabla)T\right] = \lambda_f \nabla^2 T \quad (3)$$

$$(\rho c_p)_w \left[\frac{\partial T}{\partial t} + (\mathbf{u} \cdot \nabla)T\right] = \lambda_w \nabla^2 T \quad (4)$$

Stephan correlation is used to validate the convection heat transfer coefficient of present study :

- Specified wall temperature distribution for parallel plates [Shah (1978)]

$$Nu_T = 7.55 + \frac{0.024(x^*)^{-1.14}}{1 + 0.0358(x^*)^{-0.64} Pr^{0.17}} \quad (5)$$

The mapped mesh is used in this model to solve the above system of equations. Its element size is “fine mesh”, containing 5000 elements. By performing the MATLAB code, the model is simulated to reach the steady periodic state. Then, the data processing is in the progress to figure out the heat transfer coefficient.

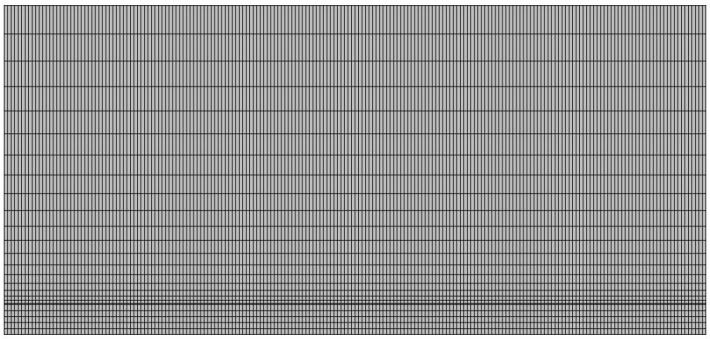

Fig. II. 2. The meshing of calculated domains

2. Results and discussion

In order to characterize h as a function of the x, simulation of conjugate heat transfer is performed using COMSOL®. Identical boundary conditions are adopted as shown in *Fig. II. 1*, and the velocity field in the flow channel is solved as well as the conduction heat transfer inside the wall. Two kinds of materials for the wall are applied, aluminum (Al) and polytetrafluoroethylene (PTFE) to compare the effect of the wall thermal conductivity. The thicknesses of the flow channel (d) and wall (z) are set as 1.2 mm and 12 mm, respectively. After the calculation reaches a steady periodic state which occurs after the 50th cycle, local values of h on the wall surface is calculated. The calculated h is compared with the value estimated using the correlation proposed by Stephan (1959) for a simultaneously developing flow between parallel plates with a constant wall temperature. The comparison of the calculated h values with those estimated using Stephan's correlation ($h_{Stephan}$) is shown in *Fig. II. 3*. The difference between h of Al wall (hAl) and $h_{Stephan}$ is found to be small, under 7% difference, except for the regions closed to the inlet of both flows ($x <$ 0.002 m and $x >$ 0.398 m for hot and cold periods, respectively). The discrepancy between hAl and h of PTFE wall (h_{PTFE}) is larger compared to the difference between

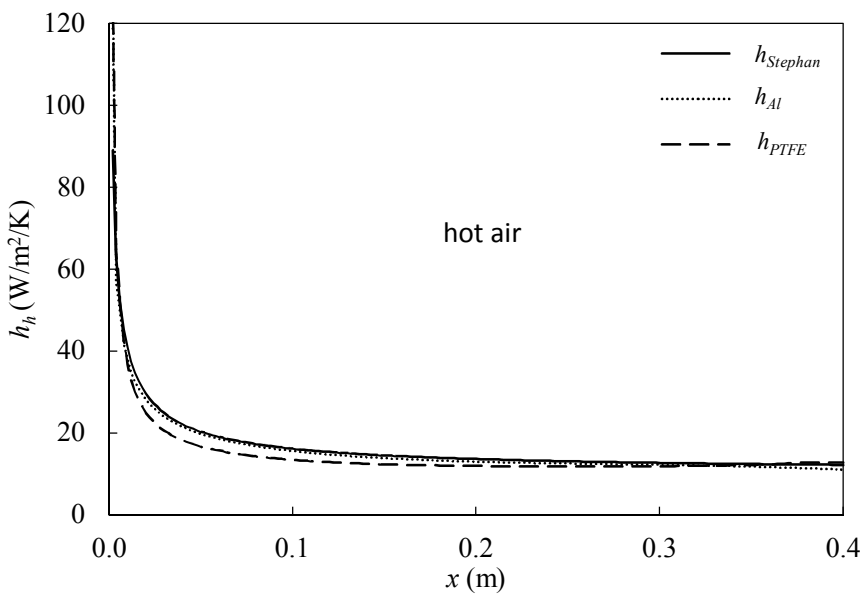

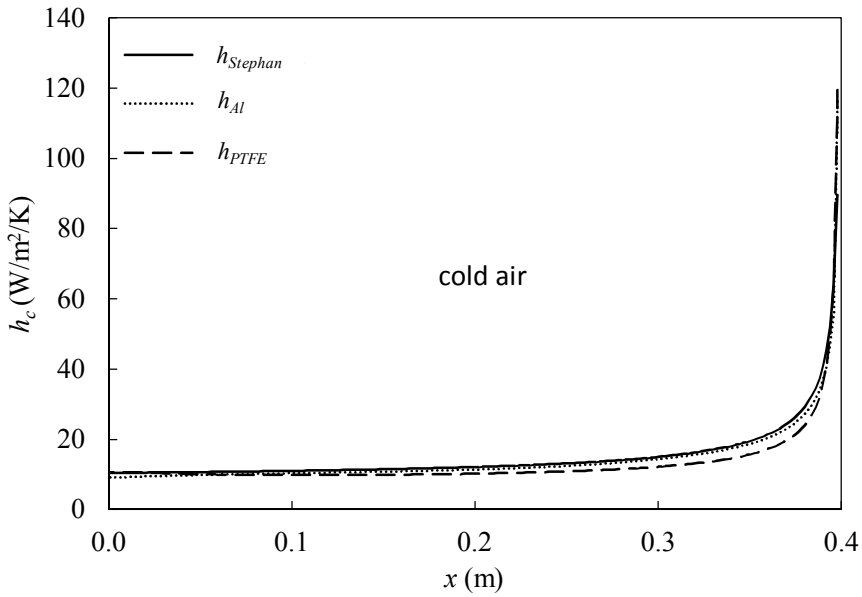

Fig. II. 3. Convection heat transfer coefficient comparison of a conjugate heat transfer calculation through COMSOL and a correlation by Stephan

h_{Al} and $h_{Stephan}$, but the average difference fall under 12% for both the hot and cold flows. The temporal changes in the h_{PEEK} depending on the location during the hot and cold periods are compared in *Fig. II. 4*. The convection heat transfer coefficient during the hot and cold periods are found to have negligible variation during the hot and cold periods. The discrepancies between h values during the hot and cold periods are observed to be smaller than 5.1% and 5.2%, respectively. Although the h values show some deviation depending on the wall material, $h_{Stephan}$ is used as the input values of h_h and h_c in equations (1) and (2). The uncertainty of the heat exchanger effectiveness calculation due to the deviation in h values are further analyzed in the result and discussion section.

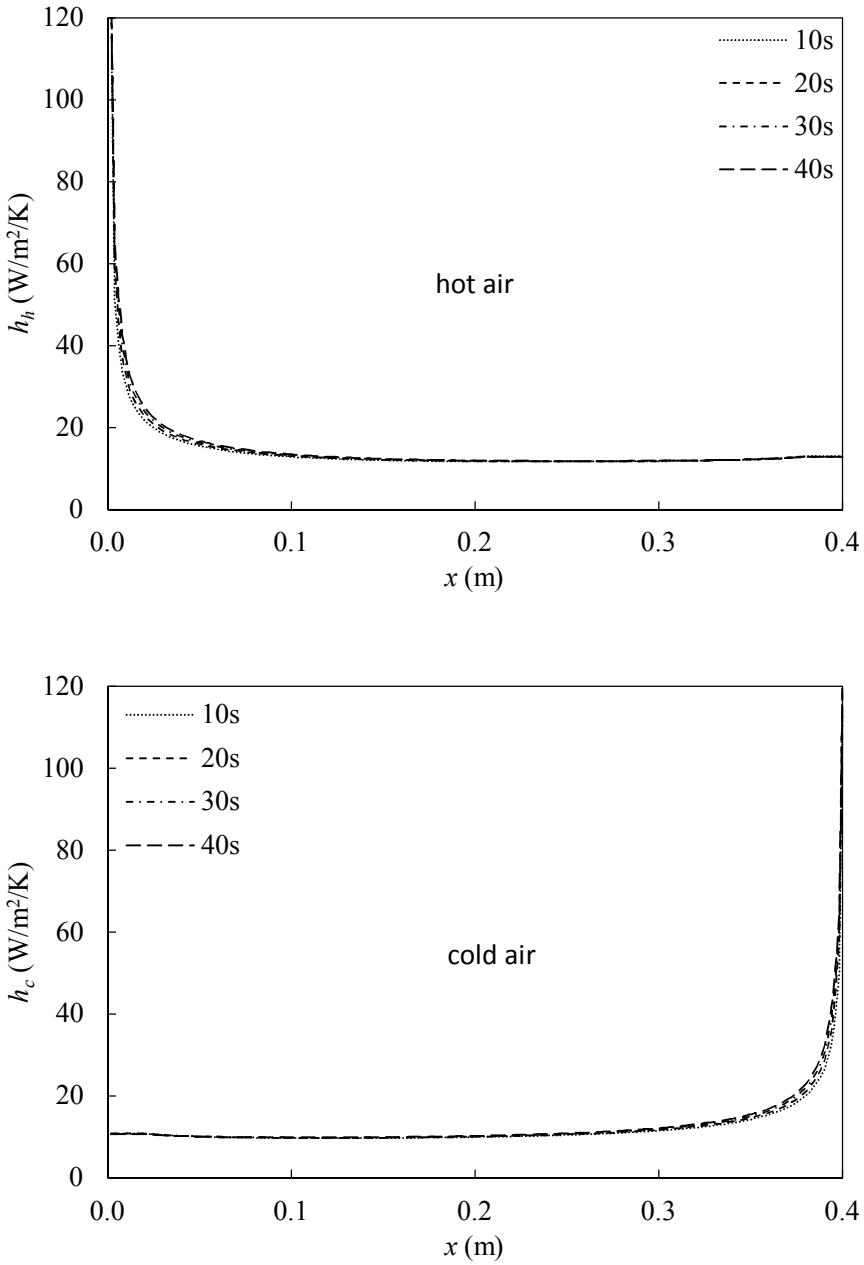

Fig. II. 4. Convection heat transfer coefficient along the x direction is shown as functions of time from the conjugate heat transfer calculation through COMSOL. The heat exchanger material is PEEK and the wall and fluid channel thicknesses are 1.2 mm and 12 mm, respectively

B. Single blow mode – solid finite conductivity

1. Plate configuration and governing equations

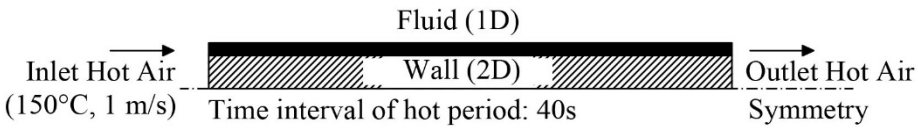

Fig. II. 5. Schematic of the calculated domains and boundary conditions

Basically, in heat transfer theory, two thermal resistances are detected between fluid and internal of heat storage. The first one is seen at the surface of heat storage and is in opposite proportion to the convection heat transfer coefficient. The another is concerned about the heat transfer from surface to inside of heat storage. In this model, assuming those resistances are equal or internal resistance is larger, temperature gradients shall be dominated in the storage material. The model is known as finite conductivity when it anticipates the transient response of thermal storage involving influences of axial and transverse conduction within material. The effects of external and internal resistances could often be related to the dimensionless parameter Bi (Biot number). If this number is small, the temperature gradients within the heat storage shall be unimportant. Inversely, transporting fluid is a liquid or when storage material owns low thermal conductivity, leading to large Bi number, an accurate estimation of the transient response of the storage could only be achieved by using finite conductivity model. However, regardless of which magnitude the Bi number is, this model which has been solved by finite difference method (FDM) is used again for validating with another numerical solution named finite element method (FEM).

The *Fig. II. 5.* describes the schematic of this single blow operating model. PTFE is chosen as a material in this calculation. Either the assumptions or the properties, operating parameters are analogous in part A. Reintroducing the governing equations of

one-dimensional energy equation for moving fluid and two-dimensional unsteady heat conduction equation for the storage material :

- Fluid domain:

$$\rho_f c_{p,f} S \left(v \frac{\partial T_f}{\partial x} \right) = h_f P (T_m - T_f) \quad (6)$$

- Wall domain:

$$\frac{\partial^2 T_w}{\partial x^2} + \frac{\partial^2 T_w}{\partial y^2} = \frac{1}{alpha} \frac{\partial T_w}{\partial t} \quad (7)$$

where $alpha$ – thermal diffusivity (m^2/s), P – heated perimeter (m), v – velocity of fluids (m/s), S – cross section are (m^2), d – wall thickness (m), T – temperature (°C), t – time (s), m - wall surface, w – interior solid, f – fluid.

Initial conditions:

$$t = 0 \qquad T_f = T_0 = 20\ ℃ \quad (8)$$

Boundary conditions:

- $x = 0 \qquad T_f = t_{f,i} = 150\ ℃$

$$\frac{\partial T_w}{\partial x} = 0, \qquad 0 < y < z \quad (9)$$

- $x = L$

$$\frac{\partial T_w}{\partial x} = 0, \qquad 0 < y < z \quad (10)$$

- $y = 0$

$$\frac{\partial T_w}{\partial y} = 0, \qquad 0 \le x \le L \quad (11)$$

- $y = \mathrm{d}$

$$k_w \frac{\partial T_w}{\partial y} = -h_f(T_m - T_f), \quad 0 \le x \le L \tag{12}$$

Dimensionless forms of this model are introduced:

$$X = \frac{x}{L};\ Y = \frac{y}{z}$$

$$V^+ = \frac{z}{L}; Fo = \frac{\alpha t}{z^2};\ G^+ = \frac{P k_m}{\dot{m}_f c_f}; T^* = \frac{T - T_0}{T_{f,i} - T_0}$$

$$Bi = \frac{hz}{k_m}$$

The transformed equations are:

- Fluid domain:

$$\frac{\partial T^*_f}{\partial X} + \frac{G^+}{V^+} Bi(T^*_f - T^*_m) = 0 \tag{13}$$

- Wall domain:

$$(V^+)^2 \frac{\partial^2 T^*_w}{\partial X^2} + \frac{\partial^2 T^*_w}{\partial Y^2} = \frac{\partial T^*_w}{\partial Fo} \tag{14}$$

Initial conditions:

$$Fo = 0 \quad T^*_f = T^*_w = 0 \tag{15}$$

Boundary conditions:

- $X = 0 \quad T^*_f = 1$ (16)

$$\frac{\partial T^*_w}{\partial X} = 0, \qquad 0 < Y < 1 \tag{17}$$

- $X = 1$

$$\frac{\partial T^*_w}{\partial X} = 0, \qquad 0 < Y < 1 \qquad (18)$$

- Y = 0

$$\frac{\partial T^*_w}{\partial Y} = 0, \qquad 0 \le X \le 1 \qquad (19)$$

- Y = 1

$$\frac{\partial T^*_w}{\partial Y} = Bi\left(T^*_f - T^*_m\right), \qquad 0 \le X \le 1 \qquad (20)$$

Nondimensional unit length:

$$\lambda = Bi\frac{G^+}{V^+} \qquad (21)$$

Nondimensional time:

$$\eta = Bi\ Fo \qquad (22)$$

❖ *Using equation – based modeling (EBM) to solve this simple model:*

Based on the simplicity of model and an assumption of constant convection heat transfer coefficient, the EBM is chosen to implement this simulation, instead of available COMSOL's module interfaces. The heat transfer coefficient applied here is estimated from Stephan correlation at the entrance region. Within the PDE (partial differential equation) interface of COMSOL, beside a number of ways to input the PDEs, coefficient form and heat equation of classical PDEs are chosen to perform this model. These forms are seen as most intuitive and simplest form to apply because each term in equation has changeable coefficients. The form of equation for a dependent variable T_f is written as:

$$e_a\frac{\partial^2 T_f}{\partial t^2} + d_a\frac{\partial T_f}{\partial t} + \nabla.\left(-c\nabla T_f - \alpha T_f + \gamma\right) + \beta.\nabla T_f + aT_f = f \qquad (23)$$

Because the equation of fluid domain is one-dimensional, ∇ is $\frac{\partial}{\partial x}$. Although the PDE formulations in COMSOL can model a variety of problems, the descriptive names for the coefficients used here that fall within the realm of continuum mechanics and mass transfer. Hence, on the left side of equal, e_a is the mass coefficient, d_a is a damping or mass coefficient, c is the diffusion coefficient, α is the conservative flux convection coefficient, β is the convection coefficient, a is the absorption coefficient, γ is the conservative flux source term. On another side, f is the source term. From the above dimensional equation of fluid domain, β is $\rho_f C_{p,f} S v$, f is $h_f P(T_m - T_f)$, and the others is 0. A general constraint which is Dirichlet boundary condition is used as inlet temperature of fluid ($T_{f,i} = r$).

The form of a dependent variable T_w is given as:

$$d_a \frac{\partial T_w}{\partial t} + \nabla.(-c\nabla T_w) = f \qquad (24)$$

where c is 1, f is 0 and d_a is $\frac{1}{alpha}$. In additions, due to the wall domain is two dimensional, there are some boundary conditions. The first one is flux source which is the place contacting directly to fluid domain:

$$-\mathbf{n}.(-c\nabla T_w) = g - qT_w \qquad (25)$$

g is $\frac{-h_f(T_m - T_f)}{k_m}$ – the boundary source term, q is 0 - the boundary absorption coefficient. The second one is zero flux meaning that those boundaries are insulated, $-\mathbf{n}.(-c\nabla T_w) = 0$.

Tab. II. 4. Calculating parameters

h (W/m².K)	88.97
d (m)	0.012
z (m)	0.001
L (m)	0.4
P (m)	1
S (m²)	0.012
k_w (W/m.K)	0.24
ρ_w (kg/m³)	2180
$c_{p,w}$ (J/kg.K)	1050
ρ_f (kg/m³)	0.8661
$c_{p,f}$ (J/kg.K)	1012.75
v_f (m/s)	0.5; 1; 1.5
$T_{f,i}$ (°C)	150
$T_{initial}$ (°C)	20
t (s)	40

2. Results and discussion

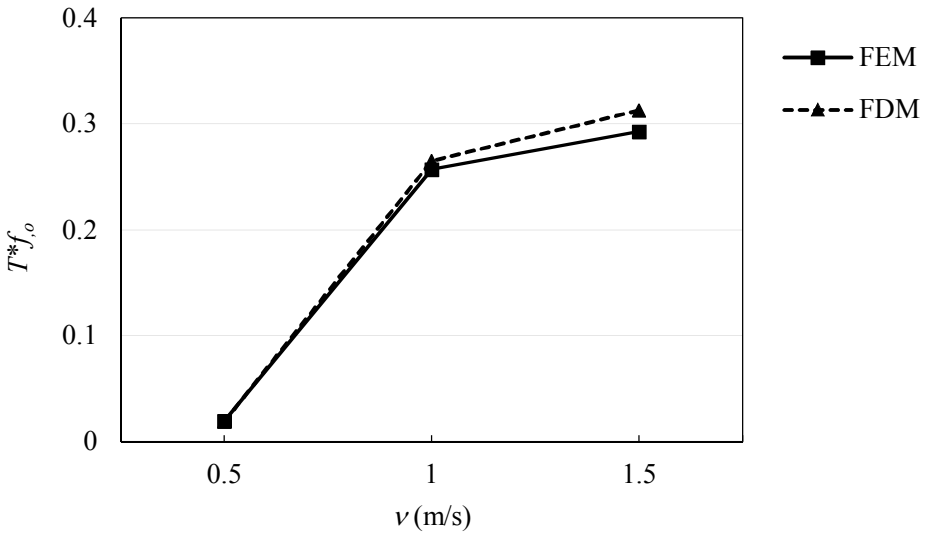

Fig. II. 6. The comparison of dimensionless outlet fluid temperature between FEM and FDM methods, with variable inlet velocity cases

The graph shows difference of single blow model which is solved by two distinct methods. In general, there are no significant distance between them, meaning that the commercial code of COMSOL is trustworthy. At inlet velocity of 0.5 m/s, the tolerance of non-dimensional outlet fluid temperature of two methods is roughly 2.9 %. By increasing the inlet velocity, the difference of results changes unremarkably, highest rate is 6.4 % happened at velocity of 1.5 m/s.

In conclusions, this simplest model of regenerator, with steady form, is used for the validation. As seen, the result is in agreement with published data of researchers, illustrating the FEM method from COMSOL can be applied correctly to estimate the thermal performance of the same but two fluid flows case, as shown in next part.

C. REGENERATIVE MODEL

1. SCHEMATIC AND GOVERNING EQUATIONS

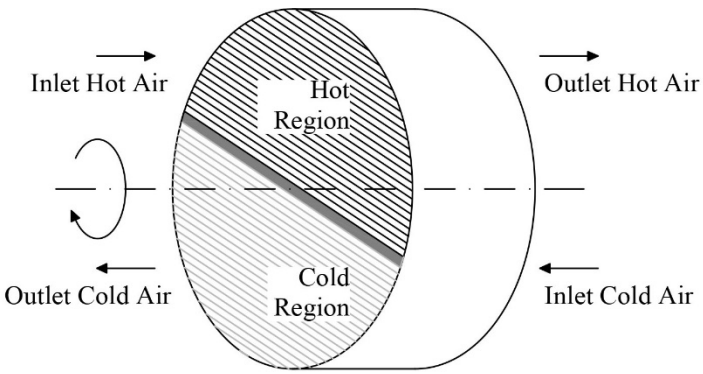

a) Rotary Regenerator

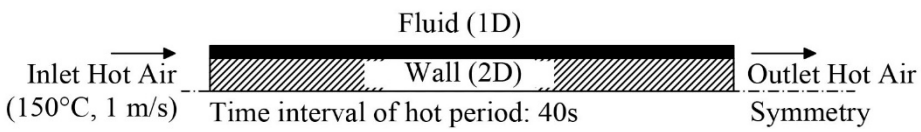

b) Hot Period

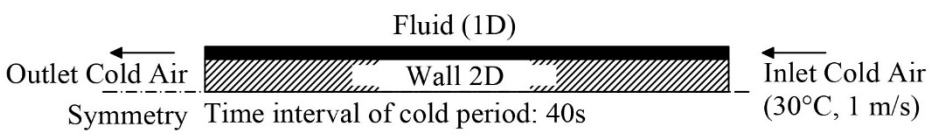

c) Cold Period

Fig. II. 7. Schematic of the calculated domains and boundary conditions

A rotary regenerator is used to recover waste heat from the exhaust gas in the boiler of thermal power plant. The rotary regenerator is shaped like a disk, and plates with clearance are packed inside the disk. A clearance produced between the plates constitutes the flow passage of the flue gas and fresh air. The disk rotates slowly (a few revolutions

per minute), and the cross-sectional circle is divided into the hot and cold regions. In the hot region, exhaust gas passes through the flow passages and simultaneously heats the matrix body. Once the matrix has been heated and moved to the cold region, an alternating fresh air is provided to the matrix. The heat contained in the matrix is released to the fresh air, and this causes heating of the fresh air before it enters the boiler. After a cycle of alternating counterflow of hot and cold fluids, the matrix walls resume their initial condition.

The schematics in *Fig. II. 7. (a)* shows a simplified rotary regenerator module. In this study, the duration of the alternating hot and cold periods is set to 40 s, each of them. During the hot period, hot air at 150 °C with velocity of 1 m/s enters the left side, as shown *Fig. II. 7. (b)*. The heat exchanger wall is heated by the air flow via convection heat transfer. After 40 s, the cold period begins. Cold air with temperature of 30 °C enters the right side at velocity of 1 m/s, as shown *Fig. II. 7. (c)*. Eventually, after numerous cycles, the module achieves a steady periodic state, i.e., a state in which the temperatures of the fluids and wall behave as a periodic oscillation.

Thermal modeling of the regenerator is divided into that on the fluid side and that on the heat exchanger material side. First, the energy conservation law is applied to the fluid side and is delineated according to the following equations for hot and cold periods, Schmidt (1983):

- Hot period:

$$\rho_h c_{p,h} S \left(\frac{\partial T_h}{\partial t} + v \frac{\partial T_h}{\partial x} \right) = h_h(x) P (T_m - T_h) \tag{26}$$

- Cold period:

$$\rho_c c_{p,c} S \left(\frac{\partial T_c}{\partial t} - v \frac{\partial T_c}{\partial x} \right) = h_c(x) P (T_m - T_c) \tag{27}$$

Here, ρ is the density, c_p is the heat capacity, A is the cross-sectional area of the flow, T is the temperature of the fluid, h is the convection heat transfer coefficient, P is the perimeter between the fluid flow and the wall surface, v is velocity of fluid, and t is the time. The subscripts h, c, and m represent the hot, cold fluids and surface of the wall, respectively. The fluids are assumed to be an ideal air. The flows are in the laminar regime, where the maximum Re is 2000. The flows considered here are categorized as simultaneously (hydrodynamically and thermal) developing flow. Therefore, the convection heat transfer coefficients vary along the x direction. Since the wall boundary conditions are neither constant temperature nor constant heat flux condition, the following investigation is performed to characterize h as a function of x and t.

The following equation can be applied as the energy equation for the conduction heat transfer inside the heat exchanger wall:

- Wall:

$$\frac{\partial^2 T_w}{\partial x^2} + \frac{\partial^2 T_w}{\partial y^2} = \frac{1}{alpha}\frac{\partial T_w}{\partial t} \tag{28}$$

Here, *alpha* is thermal diffusivity of the wall ($\lambda / \rho c_p$), λ is the thermal conductivity, and Tw represents the temperature inside the heat exchanger wall.

In theoretical modeling, the roughness and porosity of the wall are assumed to be negligible and the thermal properties of the materials are considered as constant values as shown in *Tab. II. 5*. The initial temperature of hot, cold fluids, and the wall are assumed to be 20 °C. Values of the density, heat capacity, and viscosity of the hot air, cold air, are taken as constants. The values of air properties are taken at the average temperature of hot and cold air inlet temperature of 85 °C.

The right, left, and bottom sides of the wall for both periods, are assumed to be insulated. However, on the top side of the wall, a convective boundary condition is applied for $y=d$ and $0 \leq x \leq L$ according to the following equations.

- Hot period:

$$\lambda_w \frac{\partial T_w}{\partial y} = -h_h(\mathrm{x})\,(T_m - T_h) \tag{29}$$

- Cold period:

$$\lambda_w \frac{\partial T_w}{\partial y} = -h_c(\mathrm{x})\,(T_m - T_c) \tag{30}$$

Equations (26) - (28) are coupled and solved under the boundary and initial conditions by using the partial differential equation solver, COMSOL®. In order to analyze the effects of thicknesses of the flow channel and wall on the heat transfer performance, the thicknesses of the flow channel and wall are varied from 8 mm to 18 mm and from 0.8 mm to 1.4 mm, respectively. Al, SS, CRLS, PEEK, and PTFE are considered as the heat exchanger materials. The thermal properties of the materials are listed in *Tab. II. 5*. [Usami (2004), Material Library (COMSOL 5.3a)].

Tab. II. 5. Thermal and physical properties of materials used in calculation

Material	**Density (kg/m^3)**	**Thermal conductivity (W/m/K)**	**Heat capacity (J/kg/K)**
Aluminum (Al)	2700	248	900
Stainless Steel (SS)	8000	16.2	500
CRLS	7850	44.2	450
PEEK	1320	0.25	1700
PTFE	2180	0.24	1000

Calculations are performed for 50 cycles of alternating hot and cold periods. After 50 cycles, in all cases, the difference of the heat transfer rate of hot and cold periods between consecutive cycles become smaller than 1% and a steady periodic state is achieved. The heat exchanger effectiveness (ε) in each case is calculated by the averaged outlet air temperatures of the hot and cold periods. A sensitivity analysis is performed to quantify the effects of the material thermal conductivity and thermal mass. The sensitivity

parameter S is defined as follows Costescu (2003):

$$S_{\lambda} = \frac{\partial \ln(\varepsilon)}{\partial \ln(\lambda)}, S_{\rho c_p} = \frac{\partial \ln(\varepsilon)}{\partial \ln(\rho c_p)} \tag{31}$$

The sensitivity parameter indicates the change in the effectiveness in the presence of a small fluctuation of an input parameter. For example, a small value of S_{λ} demonstrates that λ has a weak influence on the effectiveness. On the other hand, a large S_{λ} value indicates a strong influence of the input parameter on the effectiveness. Hence, the comparison of the four sensitivities (S_{λ}, $S_{\rho c_p}$) values, may provide useful information in analyzing the relative importance of design parameters on the thermal performance of the heat exchanger.

2. RESULTS AND DISCUSSION

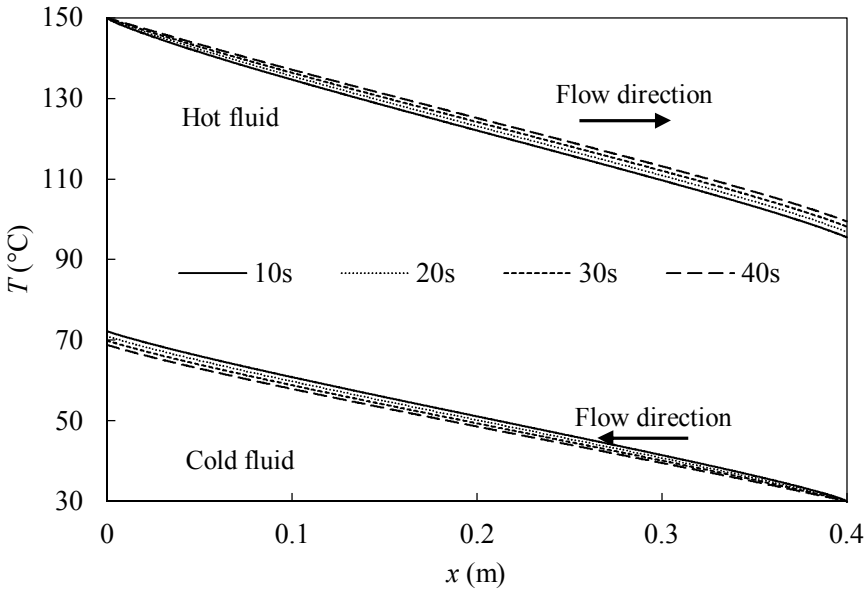

Fig. II. 8. The temperatures of the hot and cold fluids along the *x* direction is shown as function of time. The heat exchanger material is PEEK, the wall and fluid channel thicknesses are 1.4 mm and 12 mm, respectively

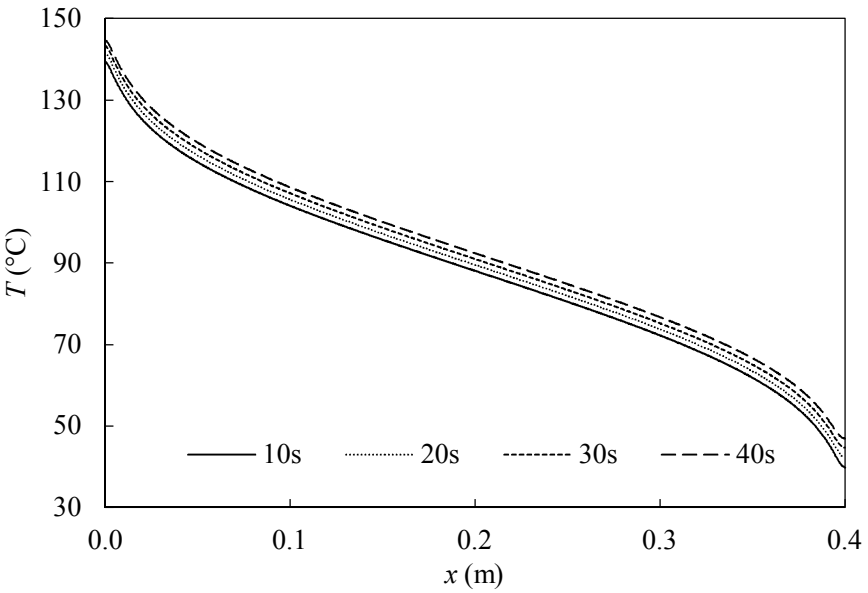

(a) Hot period

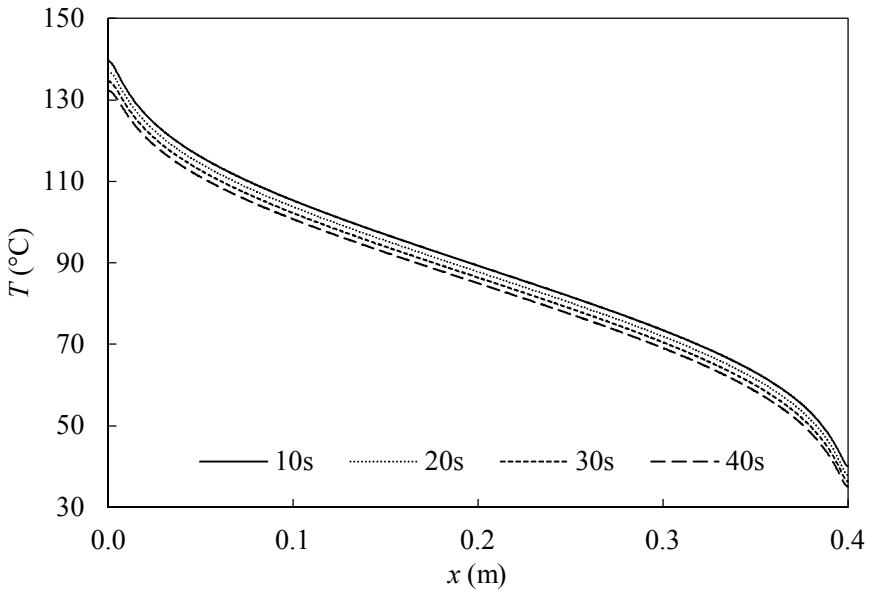

(b) Cold period

Fig. II. 9. The temperature at wall surface during the 50th cycle. The heat exchanger material is PEEK, the wall and flow channel thicknesses are 1.4 mm and 12 mm, respectively

The temperature profile in the 50th cycle of alternating hot and cold periods is shown in *Fig. II. 8.* and *Fig. II. 9.* The calculation results shown in these figures were performed with flow channel and wall thicknesses of 12 mm and 1.4 mm, respectively, and with PEEK as the wall material. The temperatures of the hot and cold fluids along the *x* direction as functions of time are shown in *Fig. II. 8.* For the hot period, the inlet air temperature is fixed at 150 °C. As hot air passes through the wall, the temperature decreases moderately and the outlet air temperature is found to range between 93.5 °C and 99.4 °C during the hot period. For the cold period, cold air with a temperature of 30 °C enters from the right side and is heated by the wall. The outlet air temperature during the cold period is calculated to range between 68.8 °C and 74.1 °C. *Fig. II. 9.* shows the temperature at the surface of the wall during the hot and cold periods at the 50th cycle. The temperature profiles of the hot and cold periods show similar curves irrespective of time. At both ends of the heat exchanger, the slope becomes steep but in

the middle section, the temperature decreases linearly along the *x* direction. The steep slope of the temperature profile at inlets of the both fluids are attributed to large *h* values in the entrance region of hot and cold fluids. The temperature on the wall surface does not change much, only by 7 °C at both ends.

On the basis of the temperature calculation, the heat exchanger effectiveness is calculated by averaging the outlet fluid temperatures and heat transfer rates during the hot and cold periods. The results for Al, SS, CRLS, PEEK, and PTFE at various thicknesses of the fluid channel and wall are shown in *Fig. II. 10*. The calculation results shown in *Fig. II. 10. (a)* were obtained under a fixed wall thickness of 1.2 mm with different materials and flow channel thick- nesses. At the flow channel thickness of 8 mm, the effectiveness of the SS heat exchanger is the highest, 0.61. However, under the same condition, the effectiveness of the heat exchanger made of Al, which has the highest thermal conductivity among all materials considered, is the lowest. *Fig. II. 10. (a)* also shows that as the flow channel thickness increases, the effectiveness of the aluminum heat exchanger decreases but becomes higher than those of the other heat exchangers. Nevertheless, the values of PEEK and PTFE effectiveness are surprisingly high, even in the case of a flow channel thickness of 18 mm; for example, the effectiveness of the PTFE heat exchanger is approximately 93 % of the highest effectiveness of the Al. The results of the effectiveness at a fixed flow channel thickness of 12 mm are shown in *Fig. II. 10. (b)*. The effectiveness corresponding to the 5 materials mentioned above are calculated at wall thicknesses in the range of 0.8 - 1.4 mm. The effectiveness does not show the dependence on the wall thickness, and for all materials, the effectiveness increases by only ~3 % when the wall thickness increases from 0.8 mm to 1.4 mm. The PEEK and PTFE heat exchangers show similar effectiveness, and in all cases, the difference between the metal heat exchangers is found to be less than 7 %.

Fig. II. 11. illustrates the comparison of effectiveness between present model and *ε-NTU* method [Shah (2003)]. The results are almost analogous among all materials. The maximum difference between the theoretical value and present calculation is found to

be 11.1% for SS. However, for PTFE and PEEK the difference is small and less than 6%.

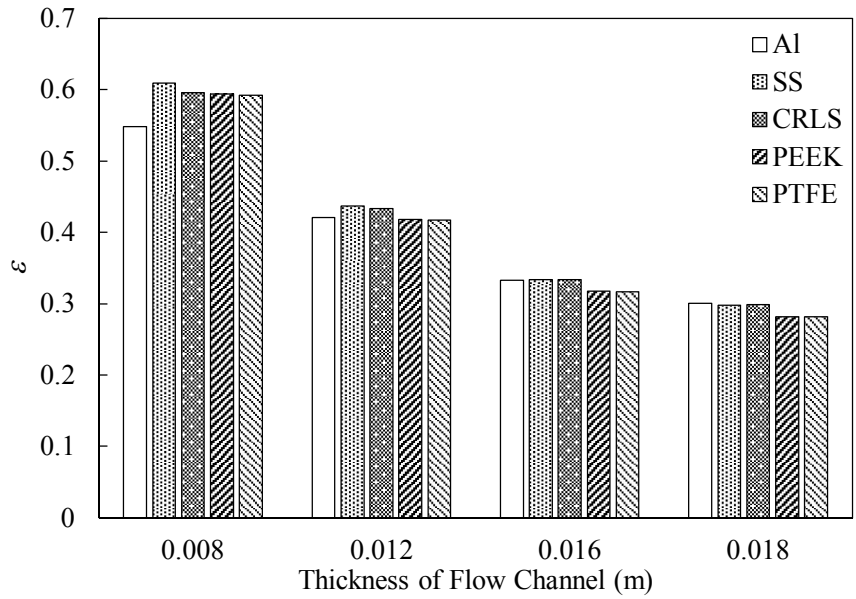

(a) The thickness of flow channel for fixed wall thickness of 1.2 mm

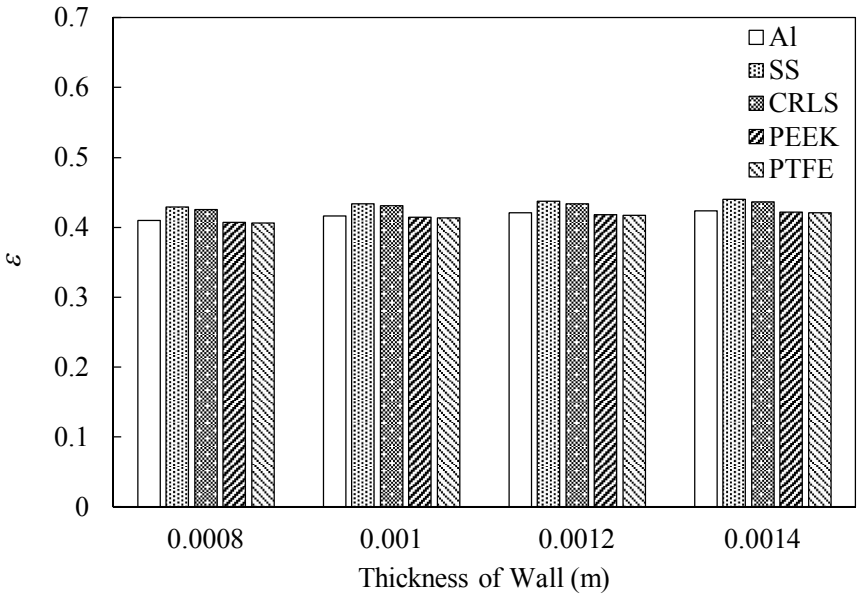

(b) The thickness of wall for fixed flow channel thickness of 12 mm

Fig. II. 10. The heat exchanger effectiveness depending on the material

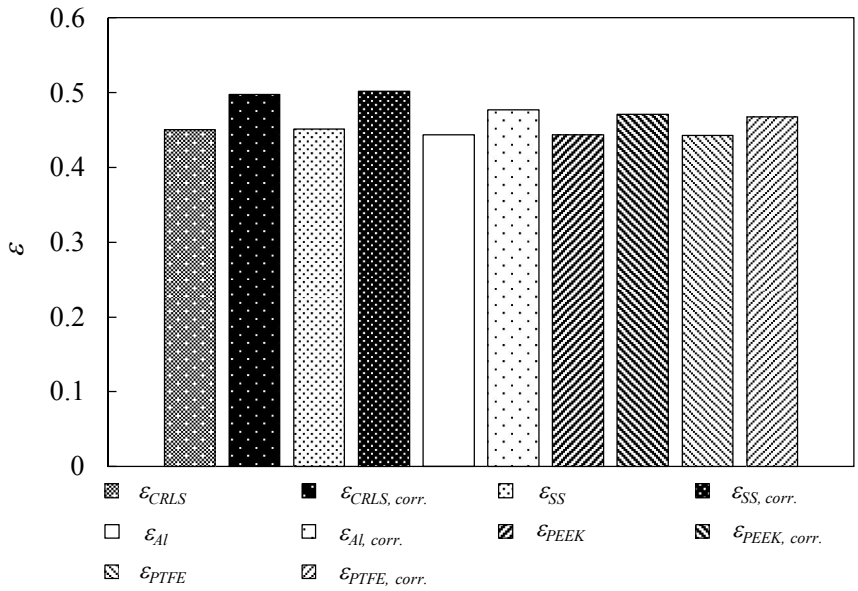

Fig. II. 11. The comparison of effectiveness between theoretical ε-NTU relation and present calculation

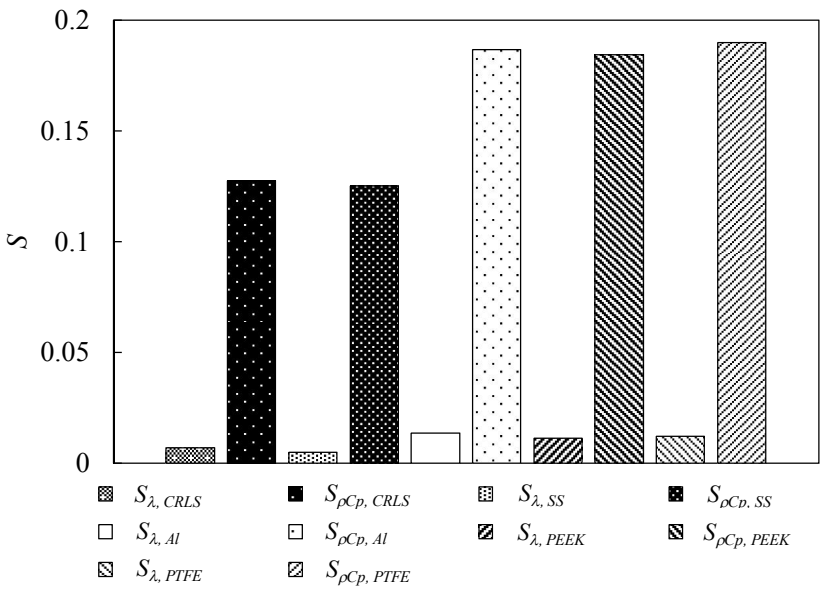

Fig. II. 12. The sensitivity of thermal conductivity and thermal mass for flow channel and wall thicknesses of 12 mm and 1 mm

The reason for the discrepancy between theoretical and calculated values is not clear. However, it is partly due to the method of calculating the average exit fluid temperature in the calculation model. The calculation of the 50 cycles of hot and cold periods in the present model was performed at a time step of 10 s. For this reason, the temperature change during a single period (40 s) was calculated as the average temperatures obtained at interval of 10 s. Since the temporal change of the outlet fluid temperature is not linear, an average temperature from a coarse time step should have some error compared to the actual value. The error in averaging the outlet fluid temperature is propagated to the total heat transfer rate and the effectiveness calculations and deviates its result to the theoretical value. The error appears to be relatively large in metals with greater total heat transfer rates and outlet fluid temperature variation, in contrast to polymer materials with relatively smaller total heat transfer rate and outlet fluid temperature variation. Error in the calculation of the effectiveness is also caused by uncertainty in h values applied in the model. As mentioned in the theoretical modeling section, h used in the current model is higher, by up to 12%, compared to the conjugate heat transfer calculation, depending on the wall material. As a result, the maximum propagated error to the calculated effectiveness value is found to be 5.3%.

Despite the existence of above mentioned uncertainties, the advantage of present model is in short calculation time compared to the full conjugate heat transfer simulation (less than 1/5). In a regenerator analysis, repeated hot and cold periods of 50 cycles need to be calculated to achieve a steady periodic state. The calculation of a single case by the conjugate heat transfer simulation may take several hours even with the current simplified geometry. However, fast and simplicity of our present model enables various calculations which may provide quantitative analysis on numerous design parameters. Through these relative comparisons, various factors affecting the effectiveness of a regenerator can be analyzed.

The sensitivity calculation results are shown in *Fig. II. 12*. The sensitivity parameter S_λ and $S_{\rho c_p}$ are calculated by using equation (31) at flow channel and wall thicknesses of 12

mm and 1 mm. The change in effectiveness caused by a 1 % change in either λ or ρc_p is calculated. For all materials, S_λ is found to be an order of magnitude smaller than $S_{\rho c_p}$. As expected, the thermal mass of the heat exchanger plays a key role in the regenerator performance than does the thermal conductivity. For the PEEK heat exchanger, 1% increase in the material thermal conductivity results in 0.02% increase in the effectiveness value. However, 1% increase in the thermal mass results in 0.18% increase in the effectiveness value. Thus, materials with larger thermal mass are more desirable than those with higher thermal conductivity.

D. Regenerative model: The conjugate heat transfer

1. Methodology

A rotary regenerator with parallel flat plate ducts has been built and simulated. These ducts (or matrix cores) compose flow channels which are arranged with fixed distances. Therefore, the modelling of fluid flows and heat transfer in a typical cell could be taken to represent for whole regenerator, as depicted in *Fig. II. 13*. For the simplicity, the 2D configuration shaped by two rectangles is chosen for this mathematical modelling. The upper one is the fluid while the another is the matrix wall. There are hot and cold periods illustrating a full rotating cycle of rotary regenerator. The hot period is set firstly at 40 second. This stage witnesses the hot flue gas enters from left side and releases its heat to the matrix wall until the end. After that, the cold period starts while the cold fresh air absorbs remaining heat from matrix wall (*Fig. II. 14*.).

The dry air is picked up as fluids to be both flue gas and cold air. From COMSOL material library, their thermo – physical properties are obtained as a function of temperature (*Tab. II. 7*.). The materials of matrix wall include Al, CRLS, PTFE, PEEK, PA6, PFA and their properties are defined in *Tab. II. 8*. The dimensions of geometry and operating conditions are also introduced in *Tab. II. 6*. The entrance region of flow channel is considered as hydrodynamically and thermally developing flow.

With the variable thickness of flow channels, their equivalent diameter is still small enough to provide denseness. Besides, the variable inlet velocity of fluid flows represents for different operating efficiencies of rotary regenerator as well as a wide range of investigated Reynold numbers. These things make the characteristics of flows become a transition zone at highest efficiency and a laminar zone at the others. Nevertheless, the turbulent model is going to be applied to predict the flow characteristics, as portrayed by Chimres (2018).

Tab. II. 6. The operating details of rotary regenerator

Parameter	Unit	Expression
L	m	0.4
d	mm	7; 8; 9; 10
Z	mm	1.2; 1.6; 2; 2.4
t_h	s	40
t_c	s	40
$T_{h,i}$	°C	150
$T_{c,i}$	°C	30
$\boldsymbol{v}_{h,i}$	m/s	10; 7.5; 5
$\boldsymbol{v}_{c,i}$	m/s	5; 3.75; 2.5

Tab. II. 7. Dry air properties

Property	Unit	Expression
μ_f	kg/m·s	$-8.38278 \cdot 10^{-7} + 8.35717342 \cdot 10^{-8}\, T^1 - 7.69429583 \cdot 10^{-11}\, T^2 + 4.6437266 \cdot 10^{-14}\, T^3 - 1.06585607 \cdot 10^{-17}\, T^4$
ρ_f	kg/m^3	$\rho_f(p_A, T), \begin{cases} \frac{\partial\left(\frac{p_A \cdot 0.02897 \cdot T}{R_{const}}\right)}{\partial p_A} \\ \frac{\partial\left(\frac{p_A \cdot 0.02897 \cdot T}{R_{const}}\right)}{\partial T} \end{cases}$
c_{pf}	J/kg·K	$1047.63657 - 0.372589265\, T^1 + 9.45304214 \cdot 10^{-4}\, T^2 - 6.02409443 \cdot 10^{-7}\, T^3 + 1.2858961 \cdot 10^{-10}\, T^4$ $(200K \le T \le 1600K)$
k_f	W/m·K	$-0.00227583562 + 1.15480022 \cdot 10^{-4}\, T^1 - 7.90252856 \cdot 10^{-8}\, T^2 + 4.11702505 \cdot 10^{-11}\, T^3 - 7.43864331 \cdot 10^{-15}\, T^4$ $(200K \le T \le 1600K)$

Tab. II. 8. Matrix wall properties

	Unit	CRLS	Al	PTFE	PEEK	PA6	PFA
ρ_w	kg/m^3	7850	2700	2180	1320	1230	2140
c_{pw}	J/kg·K	450	900	1050	1700	1700	1172
k_w	W/m·K	44.2	238	0.24	0.25	0.23	0.19

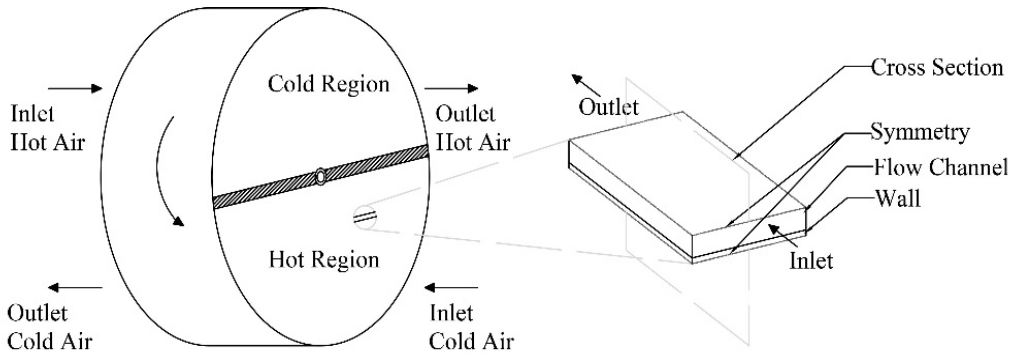

Fig. II. 13. Rotary regenerator and its section

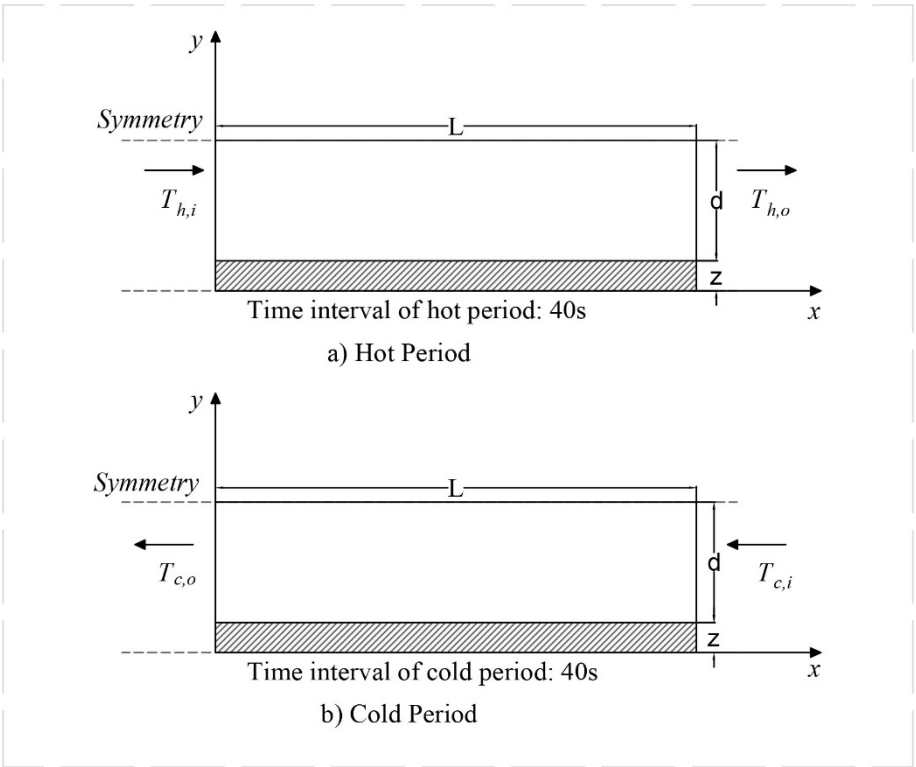

Fig. II. 14. 2D Schematic of fluid and wall domains

a. Governing equations, empirical correlations and data processing

The fluid flows are weakly compressible, meaning that their density is just evaluated at reference atmospheric pressure and is also a function of temperature. For RR, the inherent instinct for exchanging heat is transient and hence, it could not obtain totally a stationary state. Accordingly, it requires some full revolving cycles before achieving the steady periodic state – a state in which the rate of heat released from hot flue gas and then stored in matrix wall becomes analogous to that absorbed by the fresh cold air. Radiation heat transfer and rotation of RR are negligible. In spite of the flow characteristics of present study belonging to transition and laminar zones, the Reynolds averaged Navier – Stokes (RANS) turbulence type and $k-\varepsilon$ model are applied to get a better prediction (Chimres 2018). Besides, with Reynolds number is larger than 500, Sahiti (2006) figured that the laminar model could not be used to predict the flow characteristics of air flow through pin fin arrayed with pin cross - sections. Thus, the transient dimensional form of governing equations for both fluid flows are:

$$\frac{\partial \rho_f}{\partial t} + \nabla \cdot (\rho_f \mathbf{u}) = 0 \tag{31}$$

$$\rho_f \frac{\partial \mathbf{u}}{\partial t} + \rho_f (\mathbf{u} \cdot \nabla)\mathbf{u} = -\nabla \cdot \mathrm{p} + \nabla \cdot [(\mu + \mu_{\mathrm{T}})(\nabla \mathbf{u} + (\nabla \mathbf{u})^{\mathrm{T}} - \frac{2}{3}(\mu + \mu_{\mathrm{T}})(\nabla \cdot \mathbf{u})\boldsymbol{I} - \frac{2}{3}\rho_f k \boldsymbol{I} \tag{32}$$

$$\rho_f \frac{\partial k}{\partial t} + \rho_f (\mathbf{u} \cdot \nabla)k = \nabla \cdot \left[\left(\mu + \frac{\mu_{\mathrm{T}}}{\sigma_k}\right)\nabla k\right] + \mu_{\mathrm{T}}\left[\nabla \mathbf{u} : (\nabla \mathbf{u} + (\nabla \mathbf{u})^{\mathrm{T}}) - \frac{2}{3}(\nabla \cdot \mathbf{u})^2\right] - \frac{2}{3}\rho_f k(\nabla \cdot \mathbf{u}) - \rho_f \varepsilon \tag{33}$$

$$\rho_f \frac{\partial \boldsymbol{\varepsilon}}{\partial t} + \rho_f(\mathbf{u}\cdot\nabla)\varepsilon = \nabla\cdot\left[\left(\mu + \frac{\mu_{\mathrm{T}}}{\sigma_\varepsilon}\right)\nabla\varepsilon\right] + C_{\varepsilon 1}\frac{\varepsilon}{k}\left\{\mu_{\mathrm{T}}\left[\nabla\mathbf{u} : (\nabla\mathbf{u} + (\nabla\mathbf{u})^{\mathrm{T}}) - \frac{2}{3}(\nabla\cdot\mathbf{u})^2\right] - \frac{2}{3}\rho_f k(\nabla\cdot\mathbf{u})\right\} - C_{\varepsilon 2}\rho_f\frac{\varepsilon^2}{k} \tag{34}$$

$$(\rho c_p)_f\left[\frac{\partial T}{\partial t} + (\mathbf{u}\cdot\nabla)T\right] = \lambda_f\nabla^2 T \tag{35}$$

For this $k-\varepsilon$ turbulent model, constants used are $C_{\varepsilon 1} = 1.44$; $C_{\varepsilon 2} = 1.92$; $C_\mu = 0.09$; $\sigma_k = 1$; σ_ε=1.2; the turbulent viscosity is $\mu_{\mathrm{T}} = \rho C_\mu \frac{k^2}{\varepsilon}$. The analytical expressions are used to portray the flow near the wall, as known as wall function $\delta_w = \frac{\delta_w^+ \mu}{\rho u_\tau}$.

The energy equation of matrix wall is as follows:

$$(\rho c_p)_w\left[\frac{\partial T}{\partial t} + (\mathbf{u}\cdot\nabla)T\right] = \lambda_w\nabla^2 T \tag{36}$$

A sensitivity analysis is implemented to assess the effects of thermal conductivity and thermal mass. By evaluating the change of effectiveness depending on those properties, the sensitivity could supply more vital knowledges in design and improving the thermal performance of heat exchanger. Then, it is calculated by following formulas:

$$S_{\lambda_w} = \frac{\partial \ln(\varepsilon)}{\partial \ln(\lambda_w)}, S_{\rho_w c_{p,w}} = \frac{\partial \ln(\varepsilon)}{\partial \ln(\rho_w c_{p,w})} \tag{37}$$

Four correlations are used to validate the Nu number of present study :

- Specified wall temperature distribution for parallel plates, Eq. (5)
- Constant and equal wall heat fluxes: [Table 37, Shah (1978)]
- Fundamental solutions of the second kind: [Table 38, Shah (1978)]

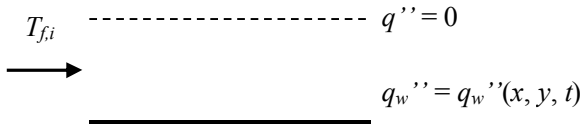

- Fundamental solutions of the third kind:

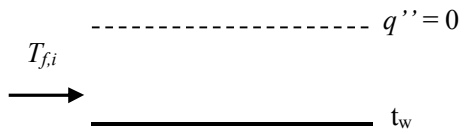

$$Nu_{3rd} = 4.86 + \frac{0.32(4x^*)^{-1.2}}{1 + 0.24(4x^*)^{-0.7} Pr^{0.17}} \tag{38}$$

At the fluid flow channel, the temperature and mass flow rate are figured out as below:

$$\overline{T_f} = \frac{1}{P_h} \int_0^{P_h} T_f(t)\, dt \tag{39}$$

Once the fluid and wall surface temperature are obtained, the local heat transfer coefficient is calculated by:

$$h_x = \frac{q_{conv}''}{\Delta T} \tag{40}$$

To validate the effectiveness of this CFD model, an analytical solution as known as ε_NTU method is applied by Razelos (Shah, 2003):

$$\varepsilon = \frac{1 - e^{\left[\frac{\varepsilon_r (C^{*2}-1)}{2C^*(1-\varepsilon_r)}\right]}}{1 - C^* e^{\left[\frac{\varepsilon_r (C^{*2}-1)}{2C^*(1-\varepsilon_r)}\right]}} \tag{41}$$

$$\varepsilon_r = \frac{NTU_{o,m}}{1 + NTU_{o,m}} \left[1 - \frac{1}{9\left(C_{r,m}^*\right)^{1.93}}\right] \tag{42}$$

$$NTU_{o,m} = \frac{2NTU_o C^*}{1 + C^*};\ NTU_o = \frac{UA}{C_{min}} \tag{43}$$

where U is overall heat transfer coefficient [W/(m^2.K)], A is total heat transfer area (m^2), C_{min} is the minimum heat capacity rate.

$$C^*_{r,m} = \frac{2C^*_r C^*}{1 + C^*} \tag{44}$$

$$C^*_r = \frac{C_r}{C_{min}} = \frac{M_w c_{p,w} N}{C_{min}} \tag{45}$$

where C^* is heat capacity ratio, M_w is the matrix mass (kg) as $Cross-sectional\ area \times Length \times Wall\ density$, N is the time interval of a regenerative cycle (s).

$$C^* = \frac{C_{min}}{C_{max}} \tag{46}$$

$$C_h = \dot{m}_h c_{p,h};\ C_c = \dot{m}_c c_{p,c} \tag{47}$$

b. Initial and boundary conditions

As the 2D modelling of RR shown in *Fig. II. 14*, the symmetry conditions are applied for the top edge of flow channel and the bottom edge of wall. The left and right sides of

$$-\mathbf{n} \cdot \mathbf{q} = 0 \tag{48}$$

matrix wall are assumed to be well insulated with adiabatic process. Hence, there are no heat fluxes across the boundaries:

The inlet of hot and cold flows has uniform and normal distribution of variable velocity (*Tab. II. D. 1. 1.*). Therefore, this flow is hydrodynamically developing flow. Due to the fact that the fluid flows come through the channel's inlet in turn, their temperature is simulated by inflow boundary condition rather than putting the uniform temperature right exactly at inlet. So, a virtual channel "upstream" is implicit and put before the

$$\mathbf{n} \cdot k\nabla T = \int_{T_{upstream}}^{T} c_p(T)dT\,\rho(T)\mathbf{u} \cdot \mathbf{n} \tag{49}$$

entrance. It is long insulated channel with given thermal properties and velocity profile at the inlet. This condition is used to define a heat flux at inlet that brings the same energy to fluid domain (noted that work done by pressure change is negligible and the flow is thermal developing flow):

Because of the small dimension, low flow rate for cold flow and large heat source for hot flow, the conductive heat flux at inlet cannot be neglected. Additionally, the inlet temperature must be modified to balance the energy yielded from the flow at inlet and energy transferred by heat conduction from the interior. Besides, the temperature boundary condition with uniform distribution could impose the inaccurate temperature value inducing the large heat fluxes which are not realistic.

Those outlet boundary conditions are relative pressure which equals to zero. For the interface between fluid flows and wall, the conditions for velocity are no slip and no

penetration. Heat fluxes, turbulent kinetic energy and turbulent dissipation rate are displayed as follows:

$$\lambda_f \left.\frac{\partial T}{\partial y}\right|_f = \lambda_s \left.\frac{\partial T}{\partial y}\right|_s ; \quad \mathbf{n} \cdot \nabla k = 0; \quad \varepsilon = \rho \frac{C_\mu k^2}{\kappa_v \delta_w^+ \mu} \tag{50}$$

The initial temperature of surrounding air as well as whole model is chosen at 25 ℃. Pressure is also atmospheric.

c. Numerical solution and validation

The governing equations of this model have been discretized using finite element method (FEM). In discretization, the linear and first – order piecewise linear interpolation are employed for temperature and pressure – velocity fields, respectively. For flat plate domains, mapped mesh has been used in the wall domain while it is free quad mesh in fluid domain. Because there is no critical change to the results of model between the element size of mesh, coarse size is chosen to calculate for all models. Time stepping is performed implicitly by backward differentiation formula (BDF) with order of accuracy varying from 1 to 2. Despite the specific distinction of FEM, it calculate directly the dependent variables in the nodes. So, a segregated approach which each of single physics is solved sequentially until reaching the convergence by direct method is applied. The termination of solving process is executed with chosen relative tolerance of 5E-3.

Fig. II. 15. illustrates the increase of Reynolds (Re) number along with the flat plate of hot flow. At highest velocity (v_h = 10m/s), the flow characteristic is in transition zone

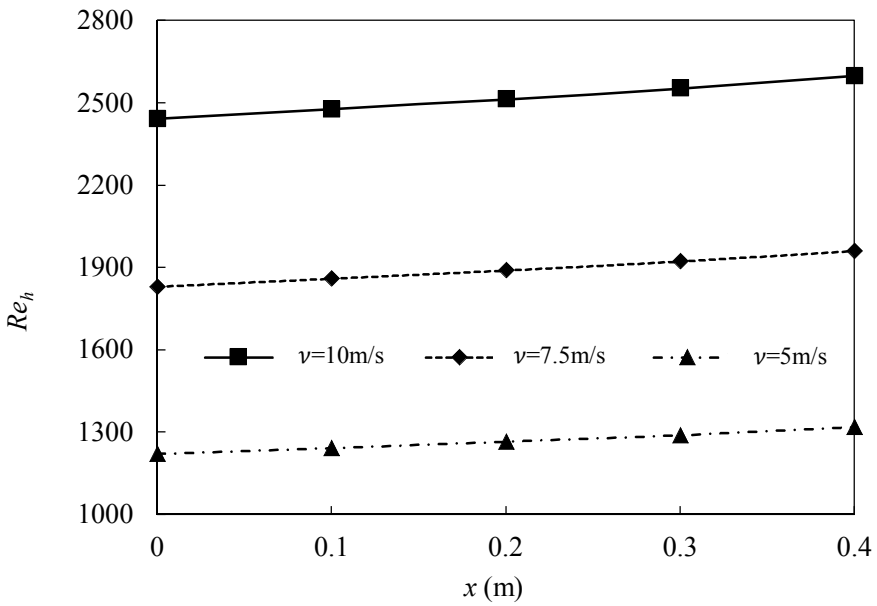

Fig. II. 15. Reynolds number as function of *x* coordinate

and those lower are in laminar zone. The flow is simulated as hydrodynamically developing flow. By the temperature dependent of thermal properties such as density, dynamic viscosity and thermal conductivity, the Re number increases along with the length of flow channel.

The validation of Nusselt number of present study is performed by comparing with the empirical correlations for PTFE flat plate case. The thickness of flow channel is 0.0035 m and PTFE wall is 0.001 m. Because of simultaneously developing flow (hydrodynamically and thermal), there are four correlations represented for four conditions such as specified wall temperature distribution (Nu_T), constant and equal wall heat fluxes ($Nu_{q''}$), fundamental solutions of the second kind (Nu_{2nd}) and third kind (Nu_{3rd}). They are applied when the flow is laminar. Therefore, in *Fig. II. 16*, the Nu number picked up from v_h = 7.5 m/s for hot flow is chosen to validate with those correlations. As shown, its values are in the area of correlations. At the entrance region, the heat fluxes are smaller than the correlations due to the aforementioned application of inflow boundary condition for inlet temperature and difference in using numerical method in this model. Nevertheless, from x of 0.04 to 0.1, the mean difference between Nu and Nu_{2nd} is 3.9 %. Starting from 0.11 to 0.2, the average rate among Nu and Nu_{3rd} is roughly 4.6 %. As seen, the Nu values stay inside the constant interval of Nu_{2nd} and Nu_{3rd}. At the beginning of 0.21, the flow gradually exits the thermal entrance region and start approaching the thermal developed flow in which the Nu number is going down to reach the Nu_T line with a range of percentage from 8.6 % to 5.4 %. It is also witnessed a steady contact of Nu value compared to $Nu_{q''}$ correlation with the average tolerance of 3.9 %.

Fig. II. 17 shows the validation between the present study and analytical solution *ε-NTU* method. The mean difference of them is approximately 6.5 %. Those typical validations show that the numerical method in this study is reliable and hence, it is used to calculate the other models with different design parameters.

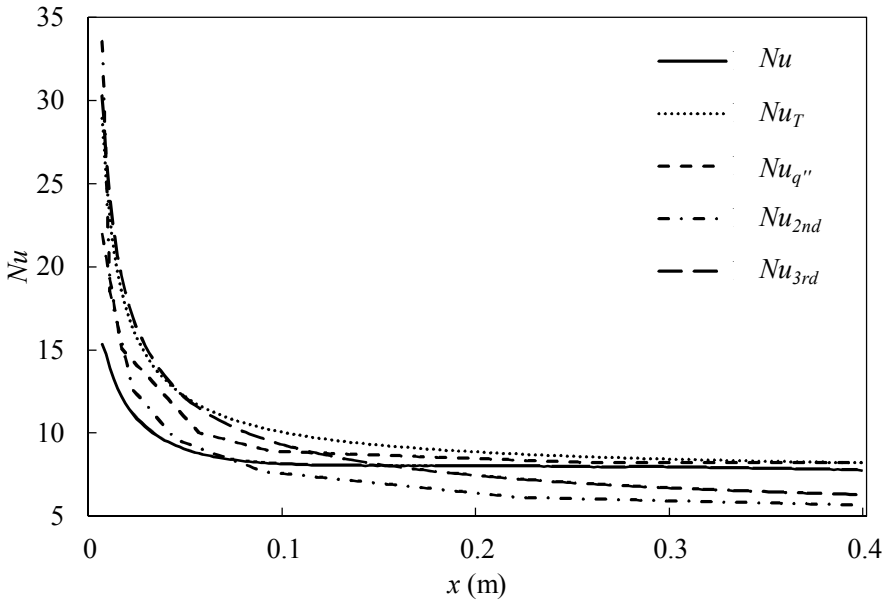

Fig. II. 16. Nusselt number as function of x coordinate

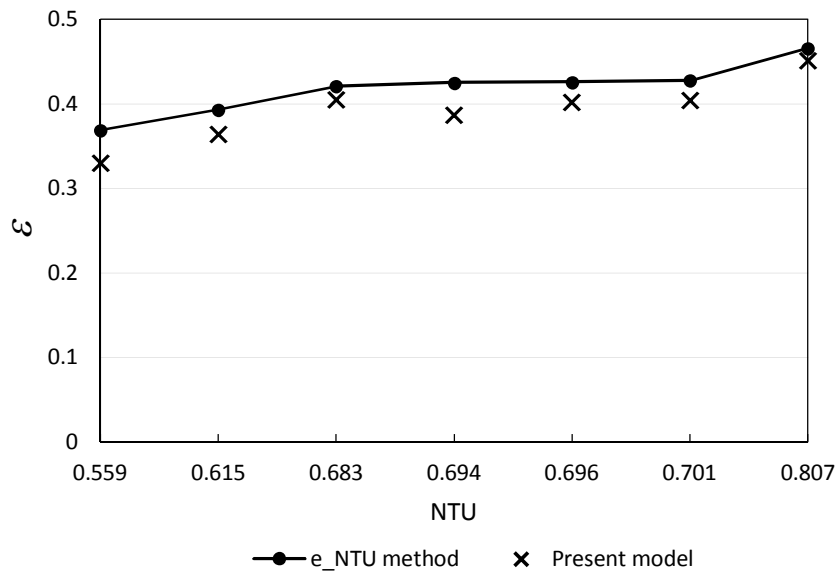

Fig. II. 17. The validation between present study and $\varepsilon - NTU$ method

2. Results and discussion

The temperature distribution and flow characteristic are shown in *Fig. II. 18* for both fluid flows – matrix wall of flat plate domains. The heat displacement is so apparent in which matrix walls absorb heat from hot fluid flow and then release it to the cold one. The arrows in the temperature figures are the energy fluxes which simultaneously describe the mass flow rate, convective and conductive heat flux of fluid flows. The distinction of flow channel and wall thicknesses is the source to create convection heat transfer coefficients which they are going to decide the heat exchanger efficiency for each material.

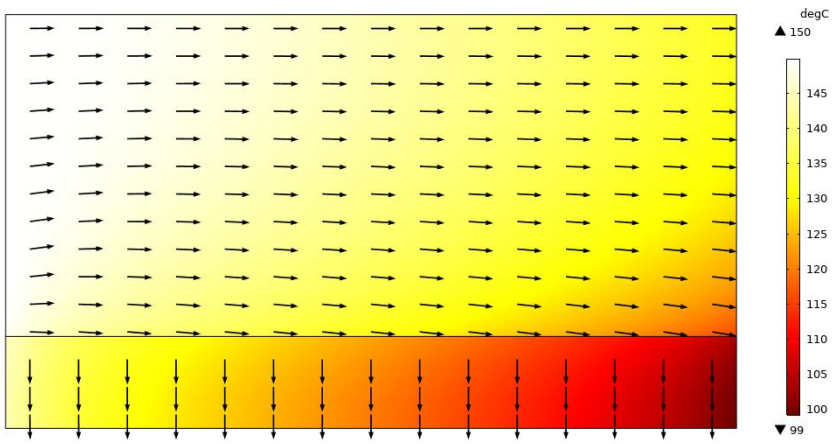

(a) The temperature profile of hot flow

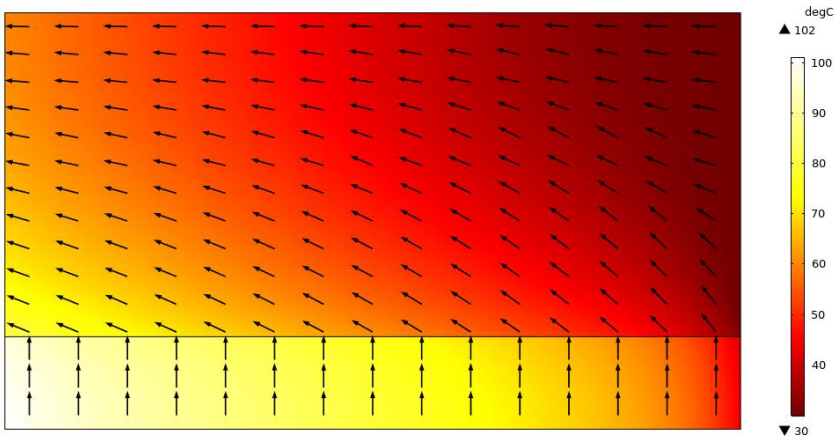

(b) The temperature profile of cold flow

Fig. II. 18. The 2D surface results of temperature of PTFE, with d = 3.5 mm and z = 1 mm

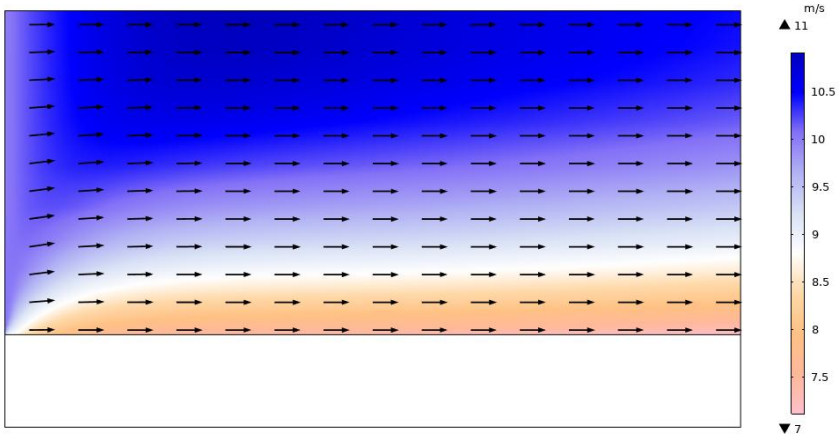

(a) The velocity profile of hot flow

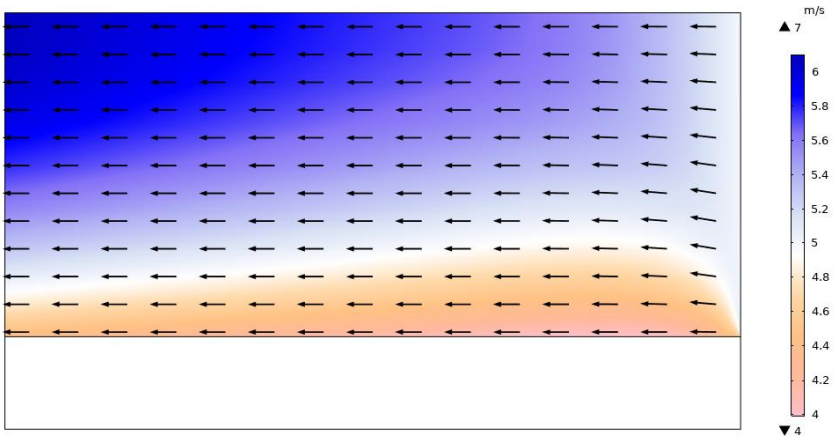

(b) The velocity profile of cold flow

Fig. II. 19. The 2D surface results of velocity of PTFE, with d = 3.5 mm and z = 1 mm

Fig. II. 20 illustrates the temperature of hot and cold flows as function of x with PTFE wall at periodic steady state. The inlet velocity of two fluid flows is 7.5 m/s and 3.75 m/s, respectively. By the time, the temperature varies physically based on what kind of flow is. For hot flow, the inlet temperature is kept continuously and constant at 150 °C after passing through the channel and transfer its heat to the matrix wall, decreases at outlet. At 0.1 s, the outlet temperature is 102.43 °C while at 10 s, it is 112.35 °C. In the end of this hot period, the outlet temperature of flow is 128.46 °C. For cold flow, the inlet temperature is also kept as constant, 30 °C. After receiving the heat stored by matrix wall at hot period, the cold flow increases its temperature at the outlet. To be continuous from hot period, at 50 s, the outlet temperature of cold flow is 84.69 °C and experiences a decline until ending a full cycle. Hence, at 80s, the temperature is approximately 66.9 °C.

After achieving the law of energy conservation within a number of cycles of heat exchanging, the following results are figured out. PTFE is picked up as a typical material to demonstrate the results as well as represent polymer rotary regenerator. First of all,

the temperature at wall surface as function of x coordinate is showed, in turn. The velocity of hot and cold flows is still 7.5 m/s and 3.75 m/s, respectively. At *Fig. II. 21* (a), because of the hot period, the walls absorb heat from the hot flow so their temperature profile tend to increase by time during the cycle. At 10 s, with a decrease from 138.5 °C to 75.56 °C along with x coordinate, its curve is quite smooth and steep thermodynamically near channel's inlet and outlet, but linear in the middle part. These things are attributed to the heat flux on heat transfer surface, thermal mass (ρc_p) of the wall. In the end of this period (40 s), the percentage ratio increases by 26.9 % compared to 0.1 s. The average temperature at 0.1 s is 90.9 °C and 124.5 °C at 40 s. For the cold period, the wall releases the heat to cold flow so temperature profile rises up by time physically. The principle is reversible to hot period, so the pattern of curves is up-side-down. At 40.1 s, the temperature of cold flow varies from 64.97 °C to 132.3 °C along the x coordinate. By the time, in the end of period (80 s), a mean decrease by 31.6 % from the beginning (40.1s) is witnessed.

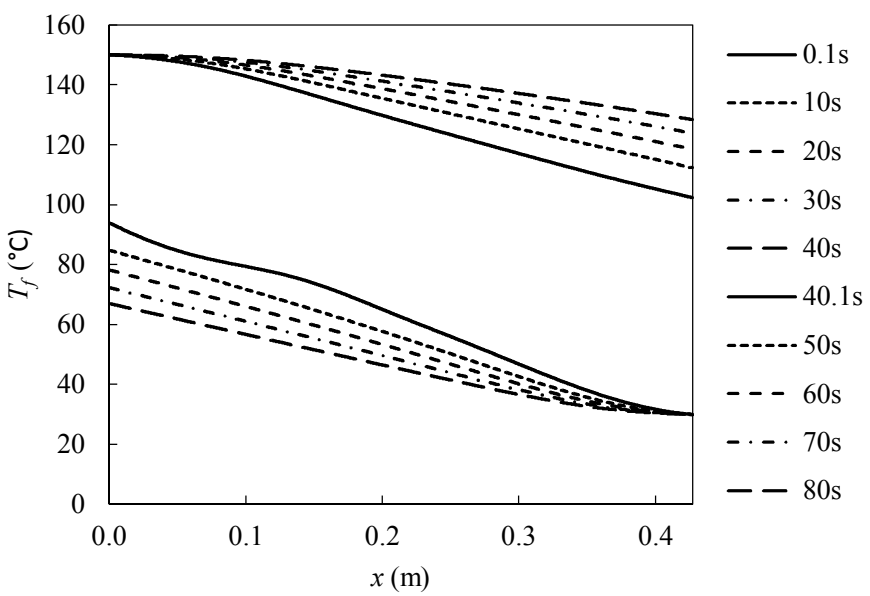

Fig. II. 20. The temperature profile of hot flow (upper) and cold flow (lower). The material is PTFE, with d = 3.5 mm and z = 1 mm

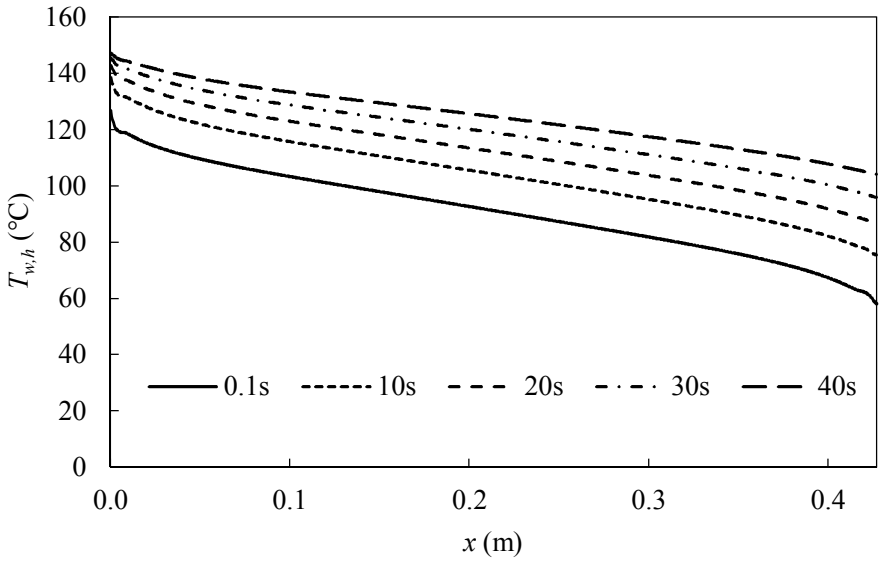

(a) Hot period

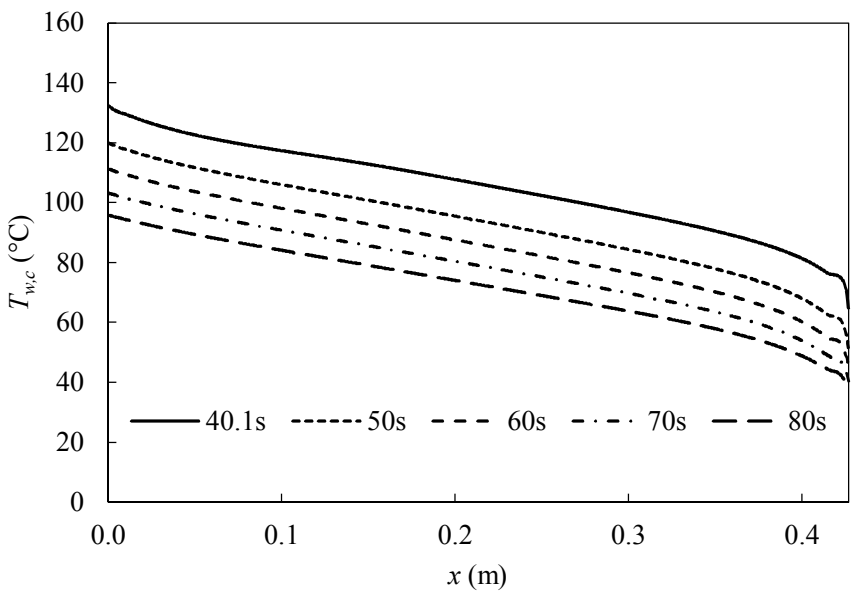

(b) Cold period

Fig. II. 21. The temperature profile at wall surface. The material is PTFE, with d = 3.5 mm and z = 1 mm

The results of heat exchanger effectiveness are calculated when the law of energy conservation is met. At *Fig. II. 22 (a)*, for each velocity profile, while keeping the uniform inlet velocity and variable flow channel thickness, the flow rate becomes different. The effectiveness values become lower generally for all materials while the thickness of fluid channel increases. For instance, the CRLS effectiveness at channel thickness of 0.0035 m is 0.445 and decreases continuously to 0.323 at 0.005 m. In spectacular, channel thickness of 0.004 is chosen to analyze. Obviously, the highest effectiveness is still CRLS with 0.398 because of inherently high thermal conductivity. Despite owning the highest thermal conductivity, the effectiveness of Al is just in the second rank, says that its capability of storing heat does not work well. For polymer materials, their results does not change significantly and almost at the same rate. The average percentage ratio of fluctuation of PEEK, PFA is 1.02 % compared to PTFE. In comparison between channel thickness of 0.004 m and 0.0045 m, its influence on effectiveness is notable. PEEK witnesses a decrease from 0.363 to 0.326, meaning that 10.14 % of reduction. A surprising observation experiences between metal and polymer.

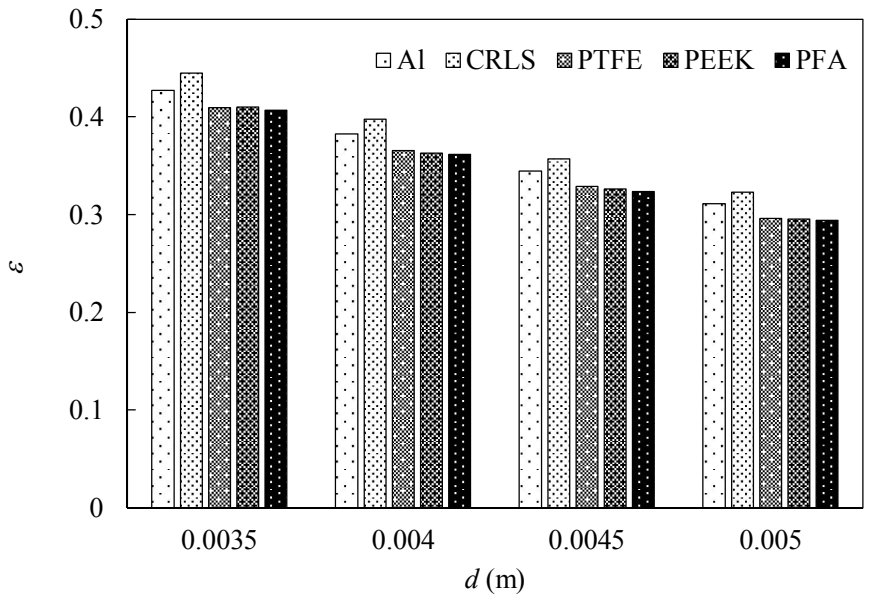

(a) The different flow rate with one velocity profile (v_h = 10 m/s, v_c = 5 m/s)

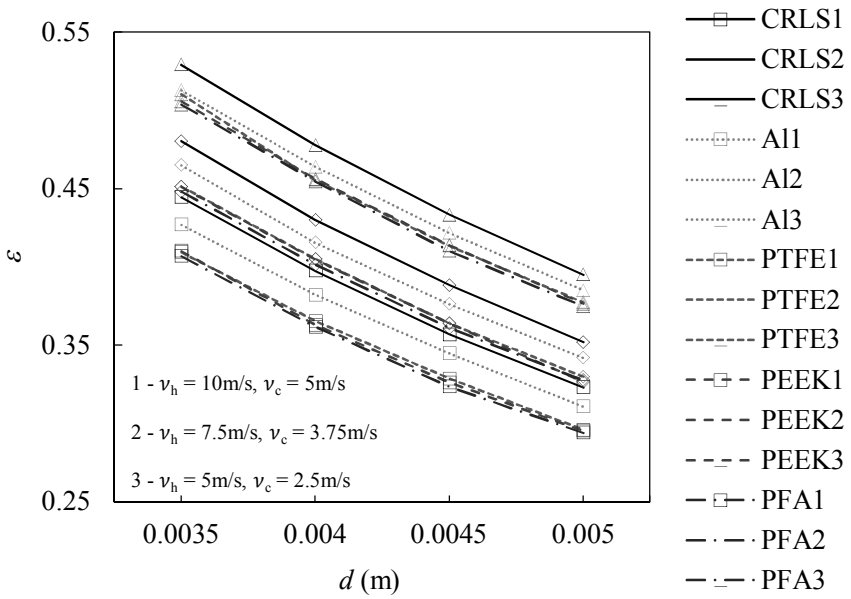

(b) 3 velocity profiles. In each profile, the different flow rate

Fig. II. 22. The effectiveness of materials with variable flow channel thickness, and 1 mm fixed wall thickness

At flow channel thickness of 0.0035 m, PTFE's effectiveness accounts for 95.9 % of Al and 92.1 % of CRLS. *Fig. II. 22 (b)* shows the effectiveness of materials with the fluctuating thickness and inlet velocity of flow channel. Generally, the higher the velocity is, the lower the effectiveness is. For instance, PFA with highest velocity experiences a lowest effectiveness range compared to the other velocity level. At channel thickness of 0.0035 m, it is 0.407 and going down to 0.294 at these of 0.005 m.

Fig. II. 23 (a) displays the effectiveness of all materials with the 1st velocity profile, changeable wall thickness and constant flow channel thickness at 4 mm. As a rule, the increment of wall thickness drives the effectiveness to enlarge, but not critical. The average percentage of an PFA's increasing between wall thickness from 0.0006 m to 0.0012 m one by one is 1.4 %. The thicker the wall is, the lower the effectiveness raises. From 0.001 m to 0.0012 m, the effectiveness just increase by 0.1% (0.3618 to 0.3623). Like the case of variable flow channel thickness above, the metals still keep the top of

heat exchanger efficiency, while polymers certainly lower and lightly oscillate each other. At wall thickness of 0.0012 m, the CRLS and PEEK is 0.4 and 0.366, respectively. *Fig. II. 23 (b)* show the same parameter of *(a)*, except the velocity profile is changeable. The lowest velocity profile (3rd) maintains the highest effectiveness compared to others of equivalent material. For example, PEEK's effectiveness at the 3rd velocity profile of 0.001 m wall thickness is 0.456, higher than 2nd profile at 11.3 % and 1st one at 20.4 %. The development of wall thickness from 0.0006 m to 0.0012 m observes a stable increment of effectiveness. Such as Al, at 0.006m and 3rd velocity profile, its value is 0.45 and keeps rising up to 0.465 at wall thickness of 0.0012 m. The average rate of this increasing is approximately 1.1 %.

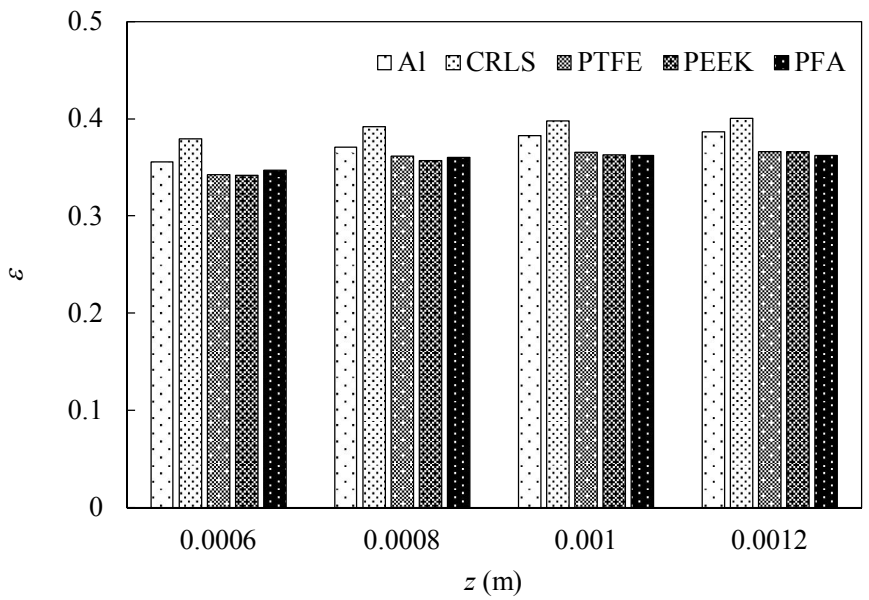

(a) The different flow rate with one velocity profile (ν_h = 10 m/s, ν_c = 5 m/s)

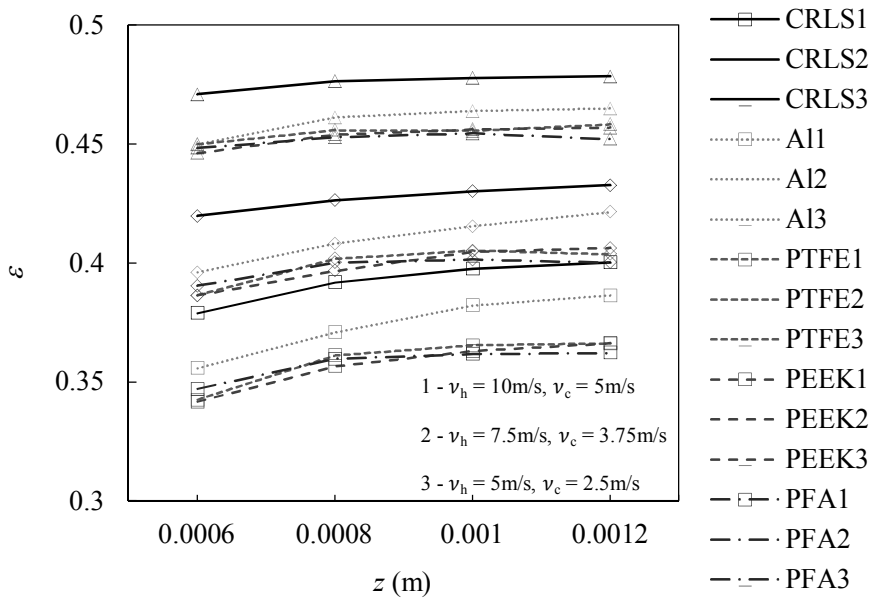

(b) 3 velocity profiles. the different flow rate

Fig. II. 23. The effectiveness of materials with variable wall thickness, and 4 mm fixed flow channel thickness

The purpose of *Fig. II. 24* is that it want to estimate the heat exchanger effectiveness of materials in case the flow rate is maintained in each velocity profile, when the flow channel thickness changes. Being different from the uniform inlet velocity of 3 profiles which is put in variable flow channel thickness (as discussed in *Fig. II. 23*), the inlet velocity of two flows is variable to keep the same flow rate. For example, the flow channel thickness of 3.5 mm and wall thickness of 1 mm, the model uses 1st velocity profile (v_h = 10m/s, v_c = 5m/s). However, as flow channel thickness increases to 4 mm – 4.5 mm – 5 mm, to maintain the same flow rate, the velocity profile at this time must be changed. At fig. (a), the general trend is that the effectiveness still decreases when thickness of fluid channel climbs up. From flow channel thickness of 3.5 mm to 5 mm, the effectiveness of CRLS experiences a diminishing steadily, roughly 19.2 %. Among materials, the thermal efficiency of metal gain the top rate while those of polymer is seen to be comparable which account for over 90 % to metal. At fig. *(b)*, the lower velocity

profile is, the higher the effectiveness of materials is. The results of polymer are analogous each other, while CRLS is still higher than Al, in all cases. Although the flow rate is kept as unchangeable, the trend of thermal efficiency of materials is still the same with the same inlet velocity or different flow rate. Similarly,

Fig. II. 25 with the same flow rate (or different inlet velocity) shows the effectiveness of variable wall thickness, at fixed flow channel. Then, three ranges of velocity are also put in the model, respectively to calculate the thermal efficiency. The less dependence on wall thickness of effectiveness in this case is recorded, for all materials.

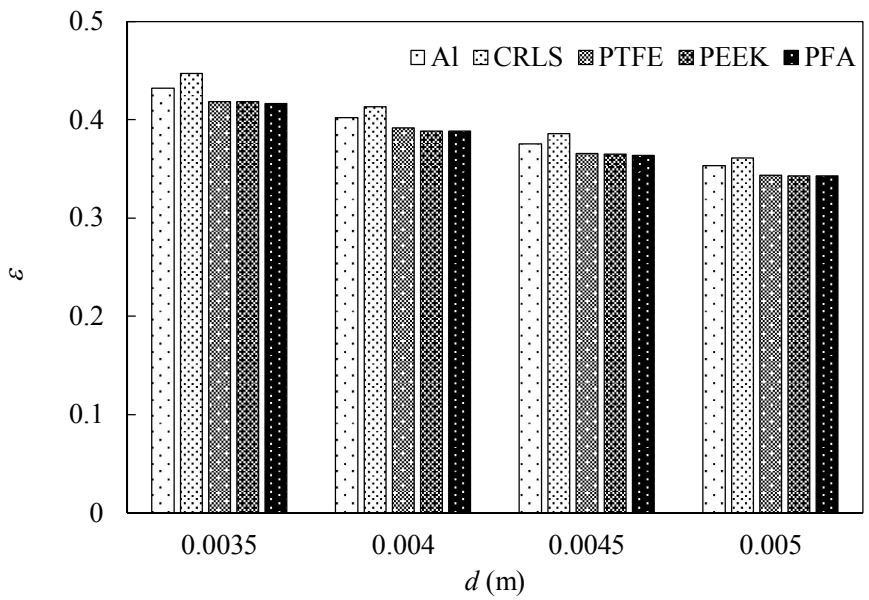

(a) The same flow rate with one velocity profile (v_h = 10 m/s, v_c = 5 m/s)

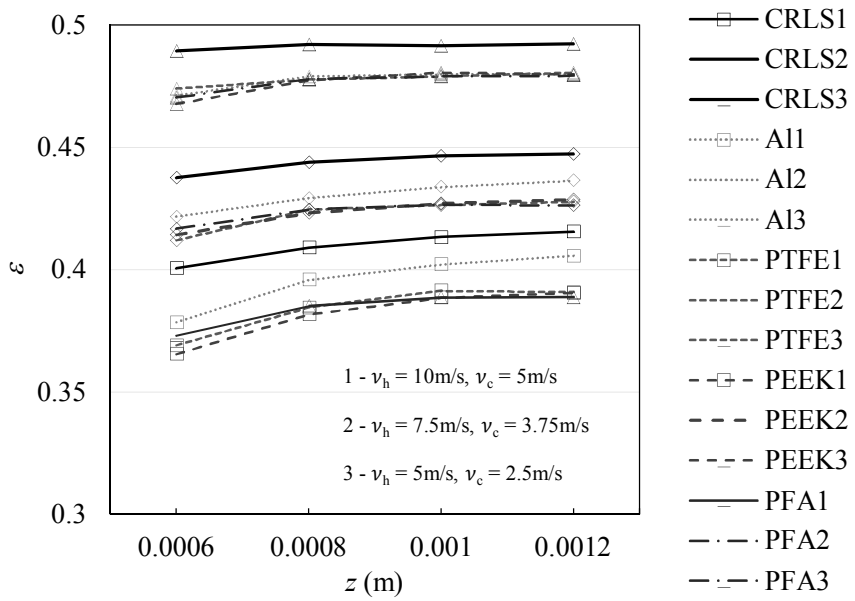

(b) 3 velocity profiles. the same flow rate

Fig. II. 24. The effectiveness of materials with variable flow channel thickness, and 1 mm fixed wall thickness

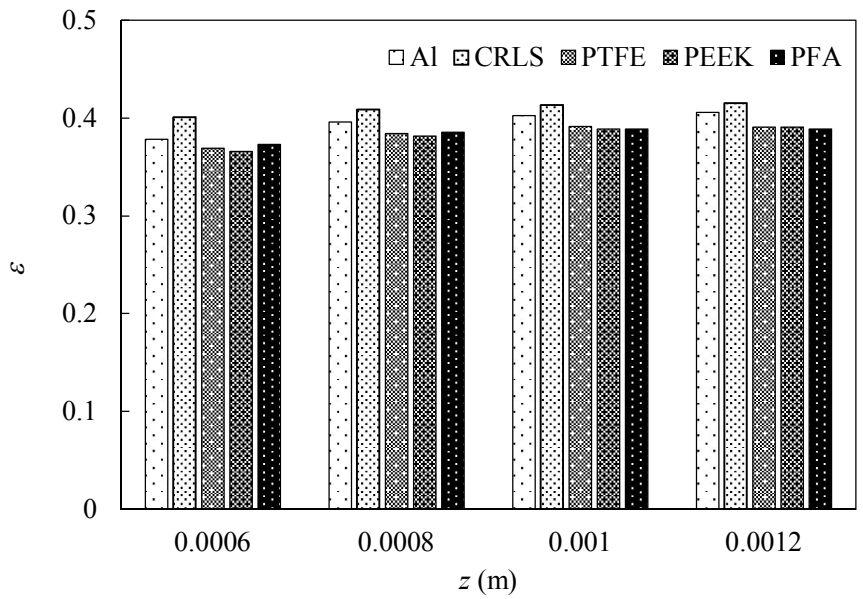

(a) The same flow rate with one velocity profile (v_h = 10 m/s, v_c = 5 m/s)

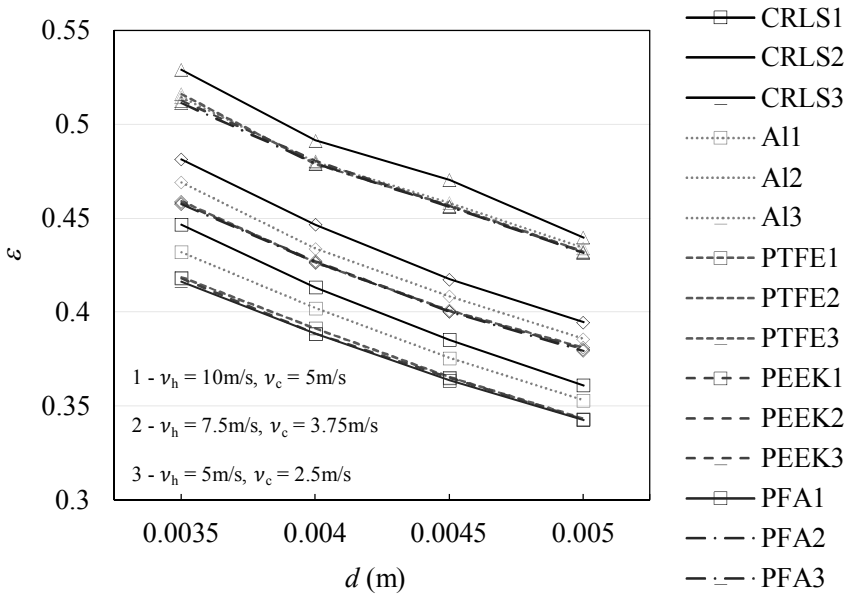

(b) 3 velocity profiles. In each profile, the same flow rate

Fig. II. 25. The effectiveness of materials with variable wall thickness, and 4 mm fixed flow channel thickness

Fig. II. 26 illustrates the comparison between two flow rate conditions. Apparently, the effectiveness of the same flow rate is better than the another one. If the same input velocity is kept when the flow channel thickness increases, the effectiveness of heat exchanger will go down. For example, PTFE of A dimension at the same flow rate has the effectiveness of 0.4186, whereas those at the different flow rate is cut down by 2.2 %.

The results of sensitivity analysis are shown in *Fig. II. 27*. The PTFE and CRLS fixed at the same flow rate, wall thickness of 1 mm and flow channel thickness of 3.5 mm are chosen to analyze the sensitivity. The modification in effectiveness generated by the increment and decrease of 5 % in either thermal conductivity or thermal mass is witnessed. In general, $S_{\rho c_p}$ occupies the highest rates whereas the S_λ stays reversely. For example, PTFE has the percentage of $S_{\rho c_p}$ which is 0.1922, higher than S_λ by 47.9 %.

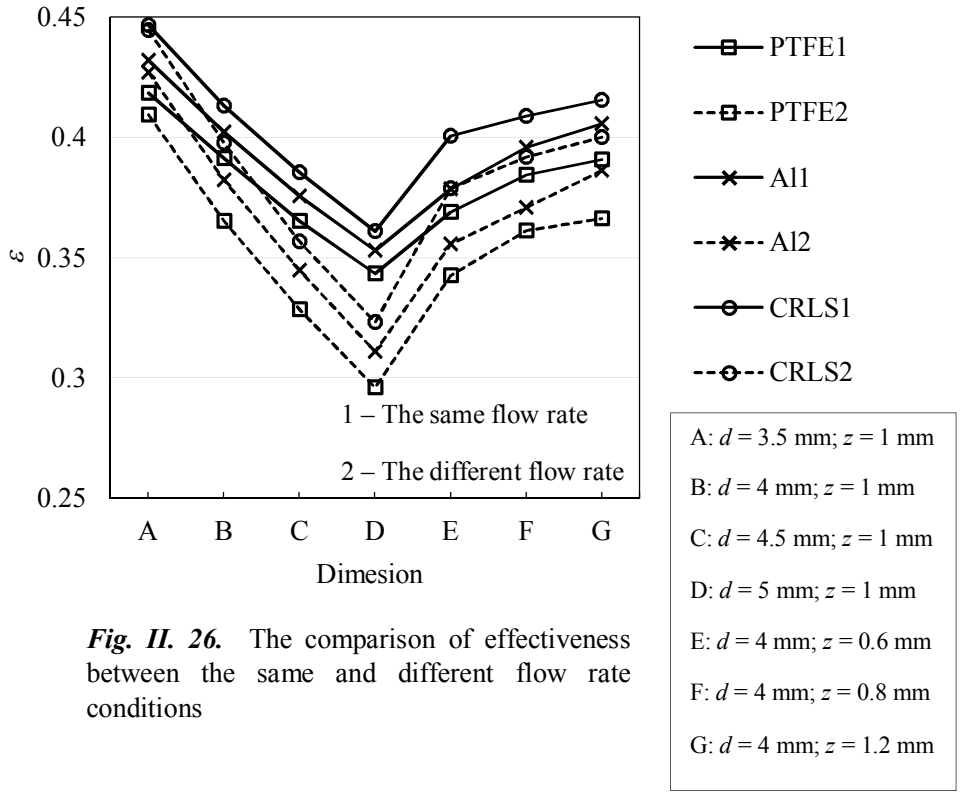

Fig. II. 26. The comparison of effectiveness between the same and different flow rate conditions

Hence, for regenerative heat exchanger, materials owning high thermal mass are more suitable rather than thermal conductivity.

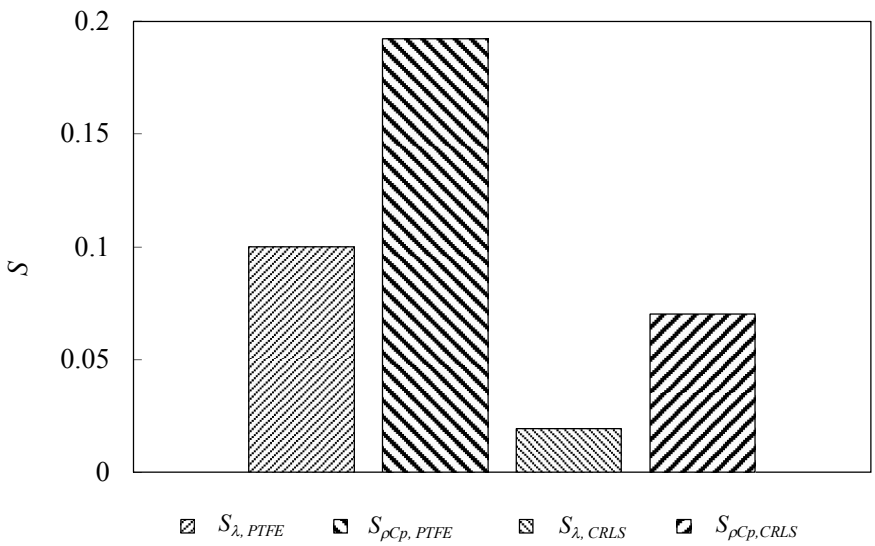

Fig. II. 27. The sensitivity analysis of thermal conductivity and thermal mass of PTFE and CRLS materials

Fig. II. 28. aims to compare the effectiveness results of the simplified and conjugate heat transfer models. The effectiveness of conjugate model is higher than the another around 24%. This happened due to the different assumptions used for the calculation. Thermal properties of fluid flows are dependent on temperature and they are in two – dimensional simulation. In conjugate model, the convection heat transfer coefficients are figured out after finishing the simulation, while in simplified model, they are estimated by using empirical correlation. Therefore, the conjugate heat transfer model may be more correct in estimating the thermal performance of regenerator rather than the old one. The future work for experimental study should be performed to validate the results with those numerical data.

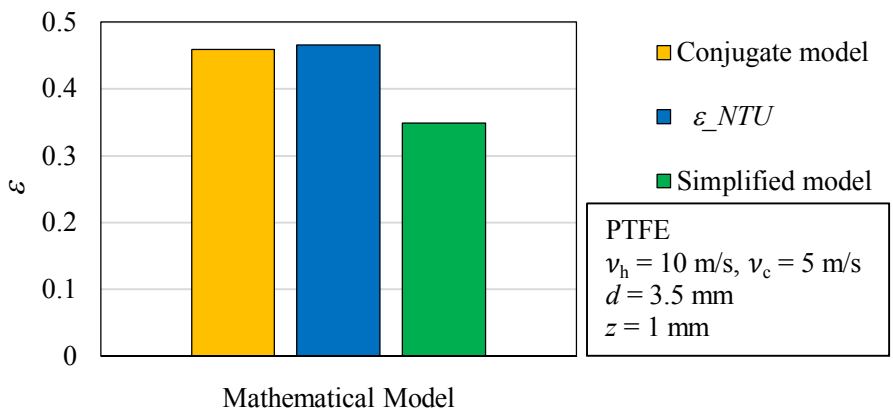

Fig. II. 28. The comparison between two mathematical models

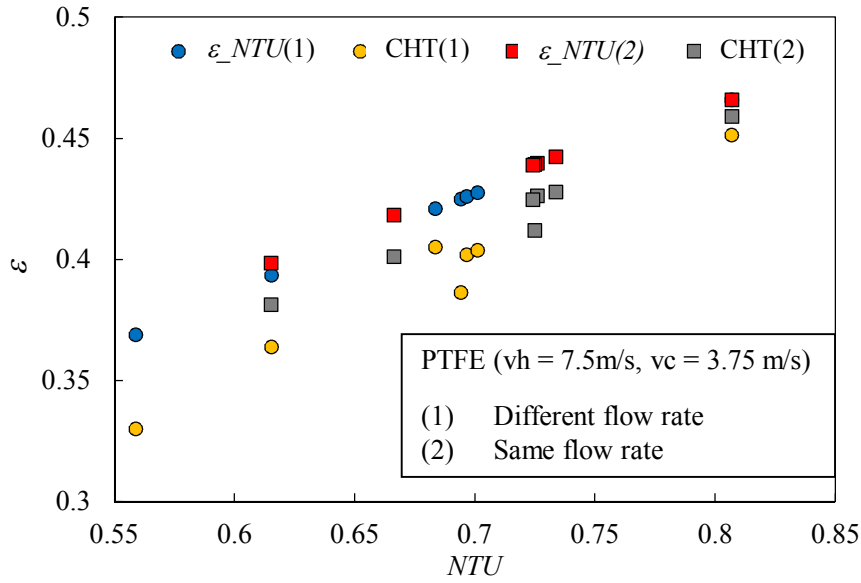

Fig. II. 29. The validation between analytical method and conjugate heat transfer model, for PTFE with two cases of flow rate

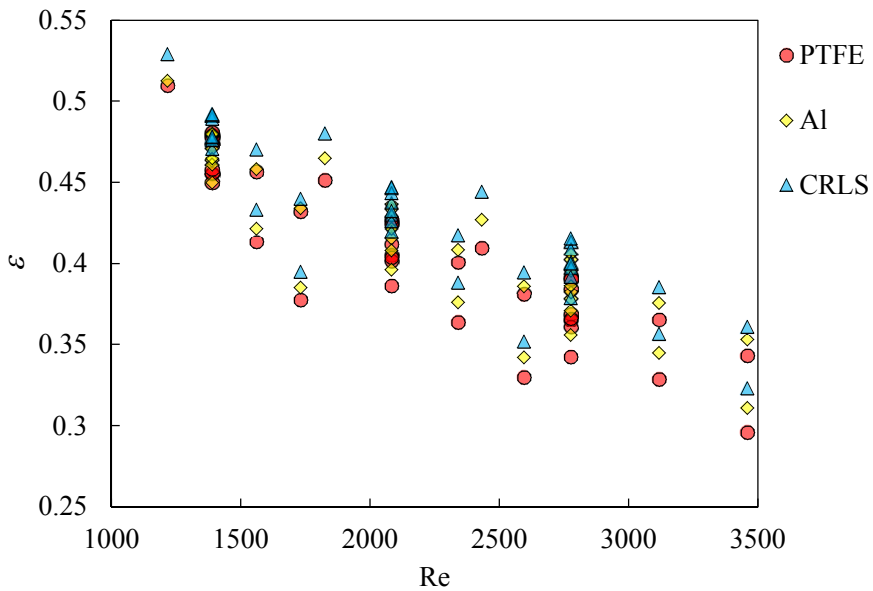

Fig. II. 30. The effectiveness of heat exchanger as function of Reynolds number of hot fluid flow

III. CONCLUSION

In this study, the thermal performance of a rotary regenerator for thermal power plant is analyzed. Governing equations of heat transfer in fluid flow on flat plate are developed and calculated for alternating hot and cold periods of thermal regenerative operation. The outlet air temperatures for the hot and cold periods are calculated after the regenerator achieves a steady periodic state, and the effectiveness values of heat exchangers made of different materials under different thickness of the flow channel and matrix wall are compared. The effectiveness values show large increment with a decrease in the flow channel thickness. However, the wall thickness has a weaker influence on the heat exchanger effectiveness for all materials. Heat exchanger made of technical polymer such as PEEK or PTFE is found to have comparable thermal performance to those made of metal, with the polymer heat exchangers showing effectiveness values of around 90 % in most calculation cases.

The sensitivity parameters for the heat exchanger effectiveness as functions of the thermal conductivity and thermal mass are calculated. For all heat exchanger materials considered, the sensitivity parameter as a function of thermal mass is more than one order of magnitude larger than that as a function of thermal conductivity. The thermal mass can be regarded as a key parameter governing the thermal performance of a rotary regenerator. Addition of high density metal or ceramic particles to a polymeric material is expected to be beneficial for enhancing the thermal performance of a polymer regenerator - which may even surpass the performance of conventional steel materials - while providing advantages such as chemical inertness, small weight, and low manufacturing costs.

REFERENCES

Zarrinehkafsh, M. T., Sadrameli, S. M., Simulation of fixed bed regenerative heat exchangers for flue gas heat recovery, Apply Thermal Engineering 24 (2004) 373–382.

Sadrameli, S. M., Journal Renewable and Sustainable Energy Reviews 58 (2016) 462–476.

Willmott, A. J., Dynamics of Regenerative Heat Transfer, Taylor & Francis, New York , (2002).

Thulukkanam, K., Heat Exchanger Design Handbook, Taylor & Francis, Florida, (2013).

Reay, D. A. J., The use of polymers in heat exchanger, Heat Recovery System & CHP 9 (1989) 209–216.

Zaheed, L., Jachuck, R. J. J., Review of polymer compact heat exchangers with special emphasis on a polymer film unit, Apply Thermal Engineering 24 (2004) 2323–2358.

Chen, L., Li Z., Guo, Z-Y. J., Experimental investigation of plastic finned-tube heat exchangers, with emphasis on material thermal conductivity, Experimental Thermal and Fluid Science 33 (2009) 922–928.

Trojanowski, R., Butcher, T., Worek, M., Wei, G., Polymer heat exchanger design for condensing boiler applications , Apply Thermal Engineering 103 (2016) 150–158.

Smith, K. M., Svendsen, S., Development of a plastic rotary heat exchanger for room-based ventilation in existing apartments, Energy and Buildings 107 (2015) 1–10.

Shah, R. K., Sekulic, D. P., Fundamentals of Heat Exchanger Design, John Wiley & Sons, New Jersey, (2003).

Schmidt, F. W., Willmott, A. J., Thermal Energy Storage and Regeneration, Hemisphere Publishing Corporation, New York, (1981).

Stephan, -Ing., K., Wärmeübergang und Druckabfall bei nicht ausgebildeter Laminarströmung in Rohren und in ebenen Spalten, Chemie Ingenieur Technik 31 (1959) 773–778.

Material Libarary, COMSOL® 5.3a, COMSOL Inc.

Usami, A., Sakamoto, S., Kusunoki, T., Okushima, M., Nishimura, S., Kojima, K., New S-TEN™1: an innovative acid-resistant low-alloy steel, Nippon Steel Tech. Report 90 (2004), 25 – 32.

Costescu, R. M., Wall, M. A., Cahill, D. G., Thermal conductance of epitaxial interfaces, Physical Review B 67 (2003) 054302.

Kern, J., Heat transfer in a rotary heat exchanger, International Journal of Heat and Mass Transfer 17 (1974) 981 – 990.

San, J. Y., Hsiau, S. C., Effect of axial solid heat conduction and mass diffusion in a rotary heat and mass regenerator, International Journal of Heat and Mass Transfer 36 (1993) 2051 – 2059.

Nair, S., Verma, S., Dhingra, S. C., Rotary heat exchanger performance with axial heat dispersion, International Journal of Heat and Mass Transfer 41 (1998) 2857 – 2864.

Zhang, X. J., Dai, Y. J., Wang, R. Z., A simulation study of heat and mass transfer in a honeycombed rotary desiccant dehumidifier, Applied Thermal Engineering 23 (2003) 989 – 1003.

Skiepko, T., Shah R. K., A comparison of rotary regenerator theory and experimental results for an air preheater for a thermal power plant 28 (2004) 257 – 264.

Sphaier, L. A., Worek, W. M., Analysis of heat and mass transfer in porous sorbents used in rotary regenerators, International Journal of Heat and Mass Transfer 47 (2004) 3415 – 3430.

Monte, F. de, Paolo, R., Linear analysis of rapidly switched heat regenerators in counterflow, International Journal of Heat and Mass Transfer 51 (2008) 3642 – 3655.

Yamaguchi, S., Saito, K., Numerical and experimental performance analysis of rotary desiccant wheel, International Journal of Heat and Mass Transfer 60 (2013) 51 – 60.

Seo, J. W., Lee, D. Y., Kim, D. S., A simple effectiveness model for heat wheels, International Journal of Heat and Mass Transfer 120 (2018) 1358 – 1364.

Wang, L., He, Y., Tang, C., Wang, Y., Che, D., A novel design of rotary regenerative condensing heat exchanger for the dehydration from high humidity flue gas, International Journal of Heat and Mass Transfer 131 (2019) 517 – 526.

Yilmaz, T., Buyukalaca, O., Design of regenerative heat exchangers, Heat Transfer Engineering 24 (2003) 32 – 38.

Shah, R. K., Skiepko, T., Influence of leakage distribution on the thermal performance of a rotary regenerator, Applied Thermal Engineering 19 (1999) 685 – 705.

Buyukalaca, O., Yilmaz, T., Influence of rotational speed on effectiveness of rotary-type heat exchanger, Heat and Mass Transfer 38 (2002) 441 – 447.

Drobnic, B., Oman, J., Tuma, M., A numerical model for the analyses of heat transfer and leakages in a rotary air preheater, International Journal of Heat and Mass Transfer 49 (2006) 5001 – 5009.

Yadav, A., Analysis of desiccant wheel with purge sector for improving the performance using a mathematical model, International Journal of Air-Conditioning and Refrigeration 22 (2014) 1450004 (15pages).

Sanaye, S., Hajabdollahi, H., Multi-objective optimization of rotary regenerator using genetic algorithm, International Journal of Thermal Science 48 (2009) 1967 – 1977.

Raja, B. D., Jhala, R. L., Patel, V., Multi-objective optimization of a rotary regenerator using tutorial training and self-learning inspired teaching-learning based optimization algorithm (TS-TLBO), Applied Thermal Engineering 93 (2016) 456 – 467.

Wang, L., Bu, Y., Li, D., Tang, C., Che, D., Single and multi-objective optimization of rotary regenerative air preheater for coal-fired power plant considering the ammonium bisulfate deposition, International Journal of Thermal Science 136 (2019) 52 – 59.

You, Y., Huang, H., Shao, G., Hu, J., Xu, X., Luo, X., A three-dimensional numerical model of unsteady flow and heat transfer in ceramic honeycomb regenerator, Applied Thermal Engineering 108 (20160 1243 – 1250.

Ozdemir, K., Serincan, M. F., A computational fluid dynamics model of a rotary regenerative heat exchanger in a flue gas desulfurization system, Applied Thermal Engineering 143 (2018) 988 – 1002.

Dreiser, C., Bart, H. J., Falling film break-up and thermal performance of thin polymer film heat exchangers, International Journal of Thermal Science 100 (2016) 138 – 144.

Shah, R. K., London, A. L., Laminar flow forced convection in ducts: a source book for compact heat exchanger analytical data, Academic Press, (1978).

Chimres, N., Wang, C. C., Wongwises, S., Optimal design of the semi-dimple vortex generator in the fin and tube heat exchanger, International Journal of Heat and Mass Transfer 120 (2018) 1173 – 1186.

APPENDIX

❖ Matlab iterative code for model to reach periodic steady state

```
model = mphopen('PTFE1');
for i = 1 : 50
% Run study 1
   model.study('std1').run
   %%
   if i == 1
% Create the file.txt to store the calculated results and then build the interpolation functions to read these files.
      int3 = model.func.create('int3', 'Interpolation');
      int3.model('comp1');
      model.func('int3').setIndex('funcs', 'IniWallTemp',0,0);

      int4 = model.func.create('int4', 'Interpolation');
      int4.model('comp1');
      model.func('int4').setIndex('funcs', 'IniFluidTemp',0,0);

      int3.set('source', 'file');
      int4.set('source', 'file');

      M1a = fullfile(tempdir,'M1a.txt');
      int3.set('filename', M1a);
      int3.set('nargs', '2');

      M1b = fullfile(tempdir,'M1b.txt');
      int4.set('filename', M1b);
```

```
int4.set('nargs', '2');

init1a = model.physics('hteq2').feature('init1').set('twc1','IniWallTemp(x,y)');
init1b = model.physics('cb2').feature('init1').set('tc1','IniFluidTemp(x,y)');
% Plot1D
pg1 = model.result.create('pg1','PlotGroup1D');
pg1.set('data','none');
lngr1 = pg1.feature.create('lngr1','LineGraph');
lngr1.set('expr','twh1');
lngr1.set('xdataexpr','x');
lngr1.set('xdatadescr','x-coordinate');
lngr1.set('data','dset1');
lngr1.selection.set(3);
lngr1.set('innerinput','manual');
lngr1.set('solnum',[11,21,31,41]);
pg2 = model.result.create('pg2','PlotGroup1D');
pg2.set('data','none');
lngr2 = pg2.feature.create('lngr2','LineGraph');
lngr2.set('expr','th1');
lngr2.set('xdataexpr',{'x'});
lngr2.set('xdatadescr','x-coordinate');
lngr2.set('data','dset1');
lngr2.selection.set(3);
lngr2.set('innerinput','manual');
lngr2.set('solnum',[11,21,31,41]);
% Plot2D
pg3 = model.result.create('pg3',2);
surf1 = pg3.feature.create('surf1','Surface');
```

```
        surf1.set('expr',{'twh1'});
        surf1.set('colortable','Thermal');
        pg4 = model.result.create('pg4',2);
        line1 = pg4.feature.create('line1','Line');
        line1.set('expr',{'th1'});
        line1.set('colortable','Rainbow');
        line1.set('linetype','tube');
    end
    %%
 % Extracting data
    x = 0 : 0.002 : L;
    y = 0 : 2e-4 : z;
    [X,Y] = meshgrid(x,y);
    coord = [X(:),Y(:)]';
    [x1,y1,twh1a] = mphinterp(model,{'x','y','twh1'},
'coord',coord,'solnum','end','edim','domain','selection',1);

    x2 = 0 : 0.002 :  L;
    y2 = z;
    [X1,Y1] = meshgrid(x2,y2);
    coord1 = [X1(:),Y1(:)]';
    [x0,y0,th1a] = mphinterp(model,{'x','y','th1'}, 'coord', coord1, 'solnum', 'end', 'edim',
'boundary', 'selection',3);
% Open files (M1a and M1b) for writing
    fid1 = fopen(M1a,'wt');
    fprintf(fid1, '%%x y twh1\n');
    for j = 1:length(twh1a)
        if ~isnan(x1(j)) || ~isnan(y1(j))
```

```
        fprintf(fid1,'%f %f %f\n', x1(j), y1(j), twh1a(j));
    end
end
fclose(fid1);

fid2 = fopen(M1b,'wt');
fprintf(fid2,'%%x y th1\n');
for j = 1:length(th1a)
    if ~isnan(x0(j))
        fprintf(fid2,'%f %f %f\n', x0(j),y0(j),th1a(j));
    end
end
fclose(fid2);

model.component('comp1').func('int3').refresh;
model.component('comp1').func('int4').refresh;
% Run study 2
model.study('std2').run;
% Set the initial value twh1 and th1 for the next iteration of Study 1 (only once)
if i==1
    int5 = model.func.create('int5', 'Interpolation');
    int5.model('comp1');
    model.func('int5').setIndex('funcs', 'IniWallTemp1',0,0);

    int6 = model.func.create('int6', 'Interpolation');
    int6.model('comp1');
    model.func('int6').setIndex('funcs', 'IniFluidTemp1',0,0);
```

```
int5.set('source', 'file');
int6.set('source', 'file');

M1c = fullfile(tempdir,'M1c.txt');
int5.set('filename', M1c);
int5.set('nargs', '2');

M1d = fullfile(tempdir,'M1d.txt');
int6.set('filename', M1d);
int6.set('nargs', '2');

init2a = model.physics('hteq').feature('init1').set('twh1','IniWallTemp1(x,y)');
init2b = model.physics('cb').feature('init1').set('th1','IniFluidTemp1(x,y)');
% Plot 1D
pg5 = model.result.create('pg5','PlotGroup1D');
pg5.set('data','none');
lngr3 = pg5.feature.create('lngr3','LineGraph');
lngr3.set('expr','twc1');
lngr3.set('xdataexpr','x');
lngr3.set('xdatadescr','x-coordinate');
lngr3.set('data','dset2');
lngr3.selection.set(3);
lngr3.set('innerinput','manual');
lngr3.set('solnum',[11,21,31,41]);
pg6 = model.result.create('pg6','PlotGroup1D');
pg6.set('data','none');
lngr4 = pg6.feature.create('lngr4','LineGraph');
lngr4.set('expr','tc1');
```

```
        lngr4.set('xdataexpr',{'x'});
        lngr4.set('data','dset2');
        lngr4.selection.set(3);
        lngr4.set('innerinput','manual');
        lngr4.set('solnum',[11,21,31,41]);
% Plot 2D
        pg7 = model.result.create('pg7',2);
        surf2 = pg7.feature.create('surf2','Surface');
        surf2.set('expr',{'twc1'});
        surf2.set('colortable','Thermal');
        pg8 = model.result.create('pg8',2);
        line2 = pg8.feature.create('line2','Line');
        line2.set('expr',{'tc1'});
        line2.set('colortable','Rainbow');
        line2.set('linetype','tube');
    end
    %%
%Extract the temperature data (twc1, tc1)
    x3 = L : -0.002 : 0;
    y3 = 0 : 2e-4 : z;
    [X2,Y2] = meshgrid(x3,y3);
    coord2 = [X2(:),Y2(:)]';
    [x3,y3,twc1a] = mphinterp(model, {'x','y','twc1'}, 'coord', coord2, 'solnum', 'end',
'edim', 'domain', 'selection', 1);
    x4 = L : -0.002 : 0;
    y4 = z;
    [X3,Y3] = meshgrid(x4,y4);
    coord3 = [X3(:),Y3(:)]';
```

```
    [x4,y4,tc1a] = mphinterp(model, {'x','y','tc1'}, 'coord', coord3, 'solnum', 'end', 'edim',
'boundary', 'selection', 3);
% Write the data in file M1a and M1b
    fid3 = fopen(M1c,'wt');
    fprintf(fid3,'%%x y twc1\n');
    for j = 1:length(twc1a)
        fprintf(fid3,'%f %f %f\n',x3(j),y3(j),twc1a(j));
    end
    fclose(fid3);
    fid4 = fopen(M1d,'wt');
    fprintf(fid4,'%%x y tc1\n');
    for j = 1:length(tc1a)
        fprintf(fid4,'%f %f %f\n',x4(j),y4(j),tc1a(j));
    end
    fclose(fid4);
    model.component('comp1').func('int5').refresh;
    model.component('comp1').func('int6').refresh;
 %% Re-set up the Study1
    model.study('std1').feature('time').set('useinitsol', true);
    model.study('std1').feature('time').set('initstudy', 'std2');
    model.study('std1').feature('time').set('solnum', 'auto');
    model.study('std1').feature('time').set('usesol', true);
    model.study('std1').feature('time').set('notsolmethod', 'sol');
    model.study('std1').feature('time').set('notstudy', 'std2');
    model.study('std1').feature('time').set('notsolnum', 'auto');

    fprintf('End of iteration No.%d\n',i);
end
```